Cement and Concrete Composites 148 (2024) 105483

Contents lists available at ScienceDirect

Cement and Concrete Composites

journal homepage: www.elsevier.com/locate/cemconcomp

Effects of hygrothermal and natural aging on the durability of multilayer insulation systems incorporating thermal mortars with EPS and aerogel

João L. Parracha [a,b,*], Rosário Veiga [a], Lina Nunes [a,c], Inês Flores-Colen [b]

[a] LNEC, National Laboratory for Civil Engineering, Av. do Brasil, 101, 1700-066, Lisbon, Portugal
[b] CERIS, DECivil, Instituto Superior Técnico, University of Lisbon, Av. Rovisco Pais, 1049-001, Lisbon, Portugal
[c] cE3c / Azorean Biodiversity Group / CHANGE – Global Change and Sustainability Institute, University of Azores, Rua Capitão João d' Àvila, Pico da Urze, 9700-042, Angra do Heroísmo, Azores, Portugal

ARTICLE INFO

Keywords:
ETICS
Accelerated aging
Natural aging
Water resistance
Aesthetic performance
Bio-susceptibility

ABSTRACT

This study evaluated the durability of three innovative multilayer insulation systems incorporating thermal mortars with EPS aggregates and silica aerogel granules after hygrothermal accelerated aging and one year of natural aging at an urban site in Portugal. The loss of performance was assessed after the accelerated aging and every three months of natural aging using non-destructive testing. Chemical-morphological analyses were also carried out prior to and after accelerated and natural aging. Results obtained after accelerated and natural aging were compared, thus contributing towards a deeper understanding of possible synergistic effects of several degradation agents and mechanisms on the long-term durability of multilayer insulation systems. The Coffin-Manson equation showed that the accelerated aging procedure (~13 days of heat/rain cycles and 5 days of heat/cold cycles) adopted herein corresponds to approximately 11 years of natural aging in typical urban conditions. The results show a significant increase in capillary water absorption and drying capacity after aging. Extensive surface microcracking was observed after accelerated aging and after 3 months of natural aging, especially in the systems facing North. Traces of biological growth were detected on both the artificially and naturally aged systems, whereas aesthetic alterations were more pronounced in North-oriented specimens after 3 months of exposure, with significantly lower surface gloss and a darker tone. On the other hand, color change cannot be detected in the artificially aged systems ($\Delta E^*_{lab} < 2$), due to the lack of degradation agents such as pollutants or UV radiation that were not included in the accelerated aging procedure.

1. Introduction

In order to achieve a climate-neutral building stock by 2050, several directives have been implemented by the European Union aiming to minimize the energy consumption of buildings and to decrease the CO_2 emissions related to the built environment [1,2]. One of the best strategies to improve the sustainability of buildings is to increase the thermal resistance of the envelope (e.g., lowering the U-values of the external walls) [3]. In this context, innovative sustainable materials and energy-efficient constructive solutions have been designed and used in new constructions and for the thermal retrofitting of building façades in recent years. Nevertheless, reliable data on the performance and durability of these innovative solutions is still lacking and these results are of fundamental importance to increase their efficiency and sustainability.

The use of lightweight thermal insulating mortars in multilayer thermal wall systems has been increasing in the last few years, mainly due to their improved thermal performance and further advantages (e.g., the possibility of levelling uneven surfaces, gap-filling, or the lack of anchoring points) [4–6] when compared to conventional thermal insulation boards. In fact, some of these thermal mortars have also been applied in the thermal retrofitting of heritage buildings with very positive results (i.e., improving the thermal performance of the building, whilst maintaining its appearance and identity) [7,8]. Thermal mortars are formulated with several lightweight aggregates (e.g., cork [9,10], expanded polystyrene [11,12], expanded perlite [13], expanded vermiculite [14], expanded clay [15], silica aerogel [16,17], etc.), together with specific additions, thus decreasing the mortar bulk density and its thermal conductivity, but also reducing the mechanical performance. Therefore, thermal mortars should have the lowest possible thermal conductivity, without compromising the mechanical

* Corresponding author. LNEC, National Laboratory for Civil Engineering, Av. do Brasil, 101, 1700-066, Lisbon, Portugal.
E-mail address: jparracha@lnec.pt (J.L. Parracha).

https://doi.org/10.1016/j.cemconcomp.2024.105483
Received 21 July 2023; Received in revised form 30 January 2024; Accepted 17 February 2024
Available online 19 February 2024

performance and the long-term durability of the whole multilayer insulation system [18].

According to the European guideline EAD 040427-00-0404 [19], these systems are made of three distinct layers (i.e., the thermal insulating mortar, the base coat, and the finishing coat). The guideline defines test methods and requirements for the performance evaluation and durability assessment of the complete multilayer insulation system, implying that the properties of each layer need to be optimized to improve the complete system's performance. The durability is assessed considering an accelerated aging test evaluating the hygrothermal and freeze-thaw performance. However, the guideline aims only to evaluate the essential characteristics of the systems and therefore additional degradation agents such as UV radiation, environmental pollutants, or biological colonization are not considered in the document. Therefore, recognizing the main degradation agents and understanding the degradation mechanisms is paramount for the sustainable and efficient use of multilayer insulation systems. In this context, a few research studies have been recently published with the aim of assessing the durability of these innovative composite systems, mainly considering hygrothermal accelerated aging tests (i.e., temperature and moisture effects).

Maia et al. [18] proposed an innovative methodology for the durability assessment of thermal mortars applied in multilayer insulation systems designing accelerated aging cycles through numerical simulation. The authors considered the material properties, climatic conditions, and the correspondent degradation mechanisms, thus allowing the use of the procedure in different climatic zones (i.e., Zone A – cold winters; Zone B – moderate winters; and Zone C – warm winters) according to the air temperature and the solar energy intensity. Posani et al. [20] proposed guidelines for using thermal mortars in the thermal retrofitting of traditional and historic masonry walls, focusing on the hygric compatibility and using validated hygrothermal simulations. Results showed hygric compatibility for multilayer systems with $A_w \times s_d < 0.2$ kg m^{-1} h$^{-0.5}$, in which $A_w \leq 0.5$ kg/m^2 and $s_d < 2$ m. Nevertheless, the authors also proposed further experimental work to validate such recommendations.

A study by Maia et al. [21] showed lower liquid water absorption after hygrothermal aging for a multilayer insulation system incorporating a thermal mortar with silica aerogel granules, which was mainly justified by the rearrangement of the system microstructure after aging. Moreover, the results showed a significant loss of compressive and flexural strengths after aging, but also a decrease in the dynamic modulus of elasticity, possibly contributing to decrease the risk of cracking. Furthermore, Xiong et al. [22] evaluated the pore structure and the water absorption of multilayer insulation systems with an expanded perlite mortar during hygrothermal accelerated aging and observed a significant alteration of the pore structure of the rendering system. The authors concluded that capillary water absorption and vapor adsorption are mainly affected by pores with a diameter lower than 10 μm and 0.1 μm, respectively.

Other research studies have been conducted to assess the influence of various degradation agents on the performance and durability of multilayer insulation systems with thermal insulation boards. Landolfi and Nicolella [62] introduced an innovative accelerated aging method specifically designed for evaluating the long-term durability of multilayer systems with thermal insulation boards. This method integrates hygrothermal and freeze-thaw cycles, effectively simulating conditions predominantly found in Europe. The results showed an increase in water absorption after aging, while the thermal conductivity demonstrated minimal change. Slusarek et al. [63] employed hygrothermal and UV accelerated aging methods to assess the influence of thermal insulation anomalies on the overall performance of multilayer systems with thermal insulation boards. During the aging process, the authors noted surface cracking and observed an increase of the finishing coat open porosity. Furthermore, Griciute et al. [64] revealed increased capillary water absorption in multilayer systems finished with a silicate-based paint after aging, in contrast to systems with acrylic-based finishing coats. Daniotti and Paolini [65] introduced a different approach designing hygrothermal and UV cycles, incorporating weather data from Milan, Italy. The authors identified key degradation agents to be included in the optimized aging cycles, specifying their frequency and intensity. However, they also suggested additional outdoor exposure for the multilayer insulation systems to establish a meaningful correlation between natural exposure and artificial aging results.

The factors affecting the durability of multilayer insulation systems are notably diverse. Durability is affected not only by the material properties, but also by in-service environmental exposure and specific degradation agents [66]. Examples of such agents encompass water-related effects like humidity, ice, and soluble salts; mechanical impacts such as temperature variations and substrate deformation; human-related influences like vandalism and pollution; and biological factors like fungi, bacteria, and algae. Previous research studies into multilayer insulation systems indicated that most failure modes occurred when one or more environmental agents acted synergistically with water [52,67]. This underscores the importance of having a suitable and durable rendering system with long-term enhanced water-repellent characteristics. In fact, the durability of the rendering system and the compatibility between the different system components are of fundamental importance for an enhanced long-term performance of the complete multilayer insulation system.

In summary, multilayer external wall insulation systems incorporating thermal mortars with different lightweight aggregates are continuously exposed to degradation agents and anthropic factors. This leads to physical-mechanical and aesthetical anomalies which compromise the efficiency and long-term durability of these cladding systems. Hence, the effects of several degradation agents on the performance and durability of multilayer insulation systems need to be further investigated. Moreover, the possible synergistic effect of these agents at a lab-scale is not easily reproduced. Therefore, a wider investigation of the long-term (i.e., natural aging) and short-term (i.e., accelerated aging) performance evaluation should also be conducted.

This paper aims at evaluating the durability of three multilayer insulation systems (two commercially available and one in a lab prototype phase under investigation) incorporating thermal mortars with EPS aggregates and silica aerogel granules after hygrothermal accelerated aging (~13 days of heat/rain cycles and 5 days of heat/cold cycles) and one year of natural aging at an urban site in Lisbon, Portugal. The durability of these systems was evaluated after accelerated aging and during natural aging using non-destructive testing (i.e., hygric performance evaluation, aesthetic performance evaluation), biological colonization analysis and chemical-morphological analyses. By comparing the results obtained after accelerated and natural aging, the study aims to enhance the understanding of the impacts of several degradation agents and mechanisms on the long-term performance of innovative multilayer insulation systems. Given that water is recognized as one of the most detrimental degradation agents for façade coatings, the findings presented in this paper are fundamental for optimizing the efficient use of these systems. Moreover, the results can serve as a reliable dataset for conducting risk assessment analyses and simulations.

2. Materials and methods

2.1. Multilayer insulation systems

Three different multilayer insulation systems (Figs. 1 and 2), supplied by two manufacturers, were tested in this study. These systems have different thermal mortar (TM), base coat (BC) and finishing coat (FC) compositions. Table 1 presents the identification and composition of the multilayer systems following the information provided by the manufacturers. In fact, S1 and S2 are commercially available multilayer insulation systems, whereas S3 is currently in a prototype phase under investigation. The relevant properties of this latter unaged system were

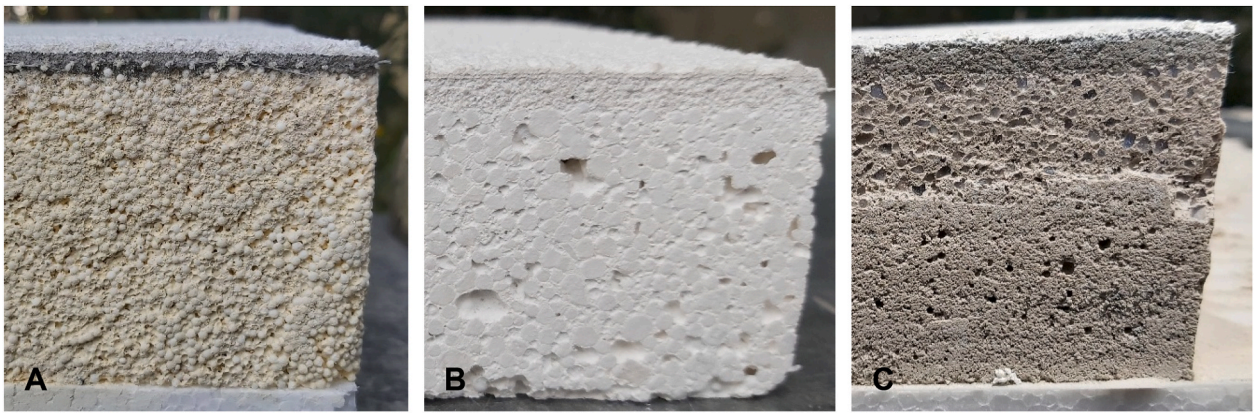

Fig. 1. Photographs of the multilayer insulation systems' boards S1 (A), S2 (B) and S3 (C) supplied by the manufacturers.

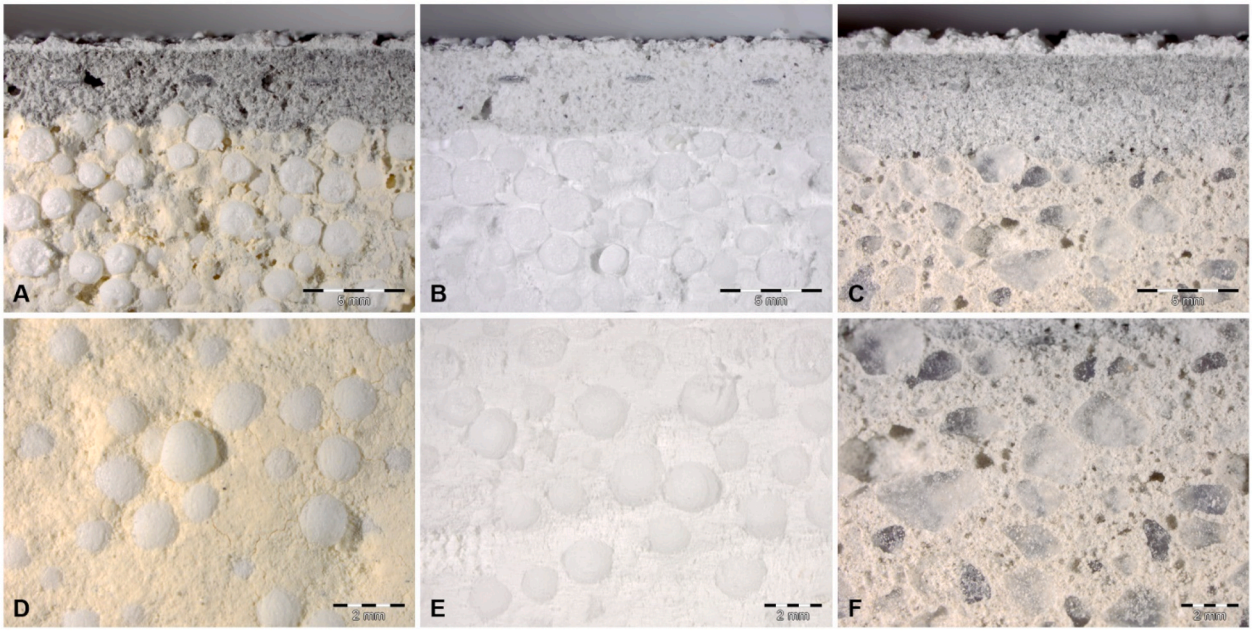

Fig. 2. Cross sections of the multilayer insulation systems S1 (A), S2 (B), S3 (C) and corresponding thermal mortars TM1 (D), TM2 (E) and TM3 (F).

Table 1
Identification and composition of the multilayer insulation systems and their components (information provided by the manufacturers or obtained in previous research [16,23]).

System (S)	Thermal mortar (TM)	Rendering system (RS)		Thickness (TM + RS) [mm]
		Base coat (BC)*	Finishing coat (FC)	
S1	Lime and EPS aggregates	Cement, mineral fillers, resins, and synthetic fibres	Acrylic-based, mineral aggregates, pigments, additives, and biocide	60.28 + 5.73
S2	Mixed binders and EPS aggregates	Cement, natural hydraulic lime, and aggregates	Acrylic-based, siloxane resin, marble powder, and biocide	37.23 + 4.52
S3	Mixed binders and silica aerogel	Cement, mineral fillers, resins, and synthetic fibres	Acrylic-based, mineral aggregates, pigments, additives, and biocide	40.50 + 5.83

* Includes a glass fibre mesh as reinforcement

Table 2
Declared characteristics of the unaged thermal insulation systems following technical datasheets (S1 and S2) or data from previous research studies (S3).

System (S)	Component	Dry bulk density [kg/m^3]	A_w [kg/(m^2.min$^{0.5}$)]	μ [−]	l [W/(m.K)]
S1*	TM1	150 ± 5	<0.4	≤5	0.042
	BC1	1200–1300	<0.2	≤20	0.45
	FC1	–	W_3**	V_2***	0.82
S2*	TM2	200 ± 50	<0.2	≤15	0.050
	BC2	1350 ± 150	<0.2	≤20	0.45
	FC2	–	W_3**	V_1***	–
S3*	TM3****	165 ± 11	1.00 ± 0.04	7.8 ± 0.1	0.029
	BC3	= BC1			
	FC3	= FC1			

* Values were determined considering the indications of EN 998–1 [24]; ** Capillary water absorption class according to NP EN 1584 [25]: $W_1 = A_w > 0.5$ kg/(m^2.h$^{0.5}$), $W_2 = 0.1 < A_w$ [kg/(m^2.h$^{0.5}$)] ≤ 0.5, $W_3 = A_w \leq 0.1$ kg/(m^2.h$^{0.5}$); *** Water vapor permeability class according to NP EN 1584 [25]: V_1 (high) = $s_d < 0.14$ m, V_2 (medium) = $0.14 \leq s_d$ [m] < 1.4, V_3 (low) = $s_d \geq 1.4$ m; **** Values collected from Pedroso et al. [16,23].

determined in previous research [16,23], with the corresponding results presented in Table 2. Moreover, Table 2 also presents the values of some properties declared by the manufacturers in the technical datasheets of systems S1 and S2.

2.2. Hygrothermal and natural aging

The three multilayer insulation systems used in this study were produced by the manufacturers as boards with an area of 1000 mm × 1000 mm. This is because we wanted to avoid any deviation of results possibly resulting from the manufacturing of the systems in our lab. The boards were then cut into smaller specimens. Three specimens of each multilayer insulation system (S1 to S3) with dimensions of 150 mm × 150 mm × thickness (Table 1) were exposed to hygrothermal accelerated aging cycles carried out in accordance with EAD 040083-00-0404 [26] guideline (Table 3). These dimensions were selected to optimize the available material and align with the reliable results obtained in previous studies by the authors (e.g., Ref. [41]) using multilayer systems with thermal insulation boards of similar dimensions. The systems were initially waterproofed on the four edges and on the backside using metallic scotch tape and silicone and then vertically fixed on a rack (~50 cm distance from the IR lamps and the sprinklers) (Fig. 3B). The accelerated aging procedure was carried out in a FitoClima 700 EDTU climatic chamber from Aralab (Fig. 3A) and consisted of: 80 repetitions of heat/rain cycles in a total of 320 h; between the heat/rain and the heat/cold cycles, specimens were left to drain for 2 h and then conditioned at a temperature between 15 °C and 25 °C and a relative humidity greater than 50% for 48 h; 5 repetitions of heat/cold cycles in a total of 120 h (Table 3).

Three specimens of each multilayer insulation system (S1 to S3) with similar dimensions to those artificially aged were naturally exposed for one year (March 2022 to February 2023) at an urban site in the campus of the National Laboratory for Civil Engineering in Lisbon, Portugal (38°45′31″N, 9°08′27″W, Altitude – 105 m). Specimens were also sealed with metallic scotch tape and silicone on the four edges and on the backside and then placed on a rack tilted 45° facing North (Fig. 3D) or South (Fig. 3C). The mean temperature, mean relative humidity, total precipitation, and mean solar radiation were registered during the exposure period using data collected from a weather station Vantage Pro2™ Plus (Davis Instruments) installed near the specimens. Fig. 4 shows the meteorological data for the exposure period. The mean temperature ranged between 11.8 °C (January 2023) and 24.9 °C (July 2022), with a total precipitation of ~1108 mm during the exposure period. It is worth noting that almost 50% of this value was obtained in the month of December 2022 (Fig. 4A), which was atypical due to the significant precipitation that occurred in Lisbon. The mean relative humidity ranged between 59% (July 2022) and 90% (December 2022) and the mean solar radiation between 50 W/m^2 (December 2022) and 302 W/m^2 (July 2022).

The specimens were identified considering their composition (Table 1), aging condition (U – unaged, HA – artificially aged, NA_N – naturally aged facing North, NA_S – naturally aged facing South) and exposure time in the case of the naturally aged specimens (3–3 months, 6–6 months, 9–9 months, 12 – one year of natural aging).

To correlate the hygrothermal accelerated aging with natural aging, and to critically analyze the relative results obtained in the two aging conditions, an acceleration factor (*AF*) was calculated using the Coffin-Manson equation (Eqs. (1)–(3)) [49,50] and considering the accelerated aging procedure of Table 3 and the meteorological data of Fig. 4. The acceleration factor (*AF*) is defined as the ratio between the reaction under accelerated aging and natural aging conditions and allows to estimate the required duration of the aging procedure to induce degradation equivalent to a reference number of years in natural weathering conditions.

$$AF_{hygrothermal\ behavior} = AF_{heat/rain} + AF_{heat/cold} \quad (1)$$

$$AF_{\frac{heat}{rain}} = \left(\frac{\Delta T_{test1}}{\Delta T_{use1}}\right)^{m_1} \quad (2)$$

$$AF_{\frac{heat}{cold}} = \left(\frac{\Delta T_{test2}}{\Delta T_{use2}}\right)^{m_2} \quad (3)$$

Regarding the heat/rain cycles (Eq. (2)), a test temperature difference (ΔT_{test1}) of 55 °C and a use temperature difference (ΔT_{use1}) of 10 °C were applied. For the heat/cold cycles (Eq. (3)), a test temperature difference (ΔT_{test2}) of 70 °C and a use temperature difference (ΔT_{use2}) of 10 °C were selected. A Coffin-Mason exponent ($m = m_1 = m_2$) equal 3 was used [51].

Acceleration factors of 166.4 and 343 were calculated considering the heat/rain and the heat/cold cycles, respectively. This would theoretically correspond approximately to 11 years of outdoor natural aging in Lisbon, Portugal (i.e., the area of natural aging). In fact, this correspondence between accelerated and natural aging should only be considered as a reference. Indeed, several uncontrolled degradation mechanisms can occur in outdoor natural conditions which are not fully represented in the accelerated aging procedure. On the other hand, accelerated aging methods are used to allow for the assessment of the long-term properties of the systems while conducting the study on a reasonable time scale. In this case, the test conditions are designed to cause substantial aging without triggering unrealistic degradation mechanisms.

Table 3
Accelerated aging procedure as defined in EAD 040083-00-0404 [26].

Hygrothermal behavior	Nr. of cycles (total h)	Test conditions
Heat/rain cycles	80 (320)	3 h at 70 ± 5 °C (10–30% RH)[a] 1 h of sprayed water (1 L/(m^2.min)) at 15 ± 5 °C
Heat/cold cycles	5 (120)	8 h at 50 ± 5 °C (≤30% RH)[a] 16 h at −20 ± 5 °C

[a] Heating is achieved using 8 thermal IR lamps of 250 W each.

2.3. Durability assessment

The durability of the multilayer insulation systems was evaluated considering a set of non-destructive tests (i.e., visual and stereomicroscope observations for the detection of surface anomalies, capillary water absorption, gloss and color, biological colonization) performed in unaged conditions, after hygrothermal accelerated aging, and each three months till one year of natural aging. The naturally aged specimens were collected from the exposure site every 3 months to be evaluated and tested in laboratory conditions where they stayed no more than a week. Additional tests involving a longer timespan or destructive assessment (i.e., water vapor permeability, drying kinetics, SEM-EDS and MIP analysis) were carried out only on the systems in unaged conditions, after hygrothermal aging, and after one year of natural aging.

2.3.1. Visual inspection and stereomicroscope observations

The external surfaces of the multilayer insulation systems were visually inspected with the help of a stereo microscope Olympus SZH10 (Olympus SC30 image acquisition system and Olympus LabSens software) to detect the presence of surface anomalies (e.g., cracks, material loss, stains).

2.3.2. Capillary water absorption and drying kinetics

The capillary water absorption of the multilayer systems was determined in a conditioned room (T = 23 ± 2 °C; RH = 65 ± 5%) according to the recommendations of EAD 040083-00-0404 guideline [26]. All specimens were previously stored in the same room for mass stabilization. The test consisted of the application of the finishing coat of each system in direct contact with the water, ensuring total submergence of

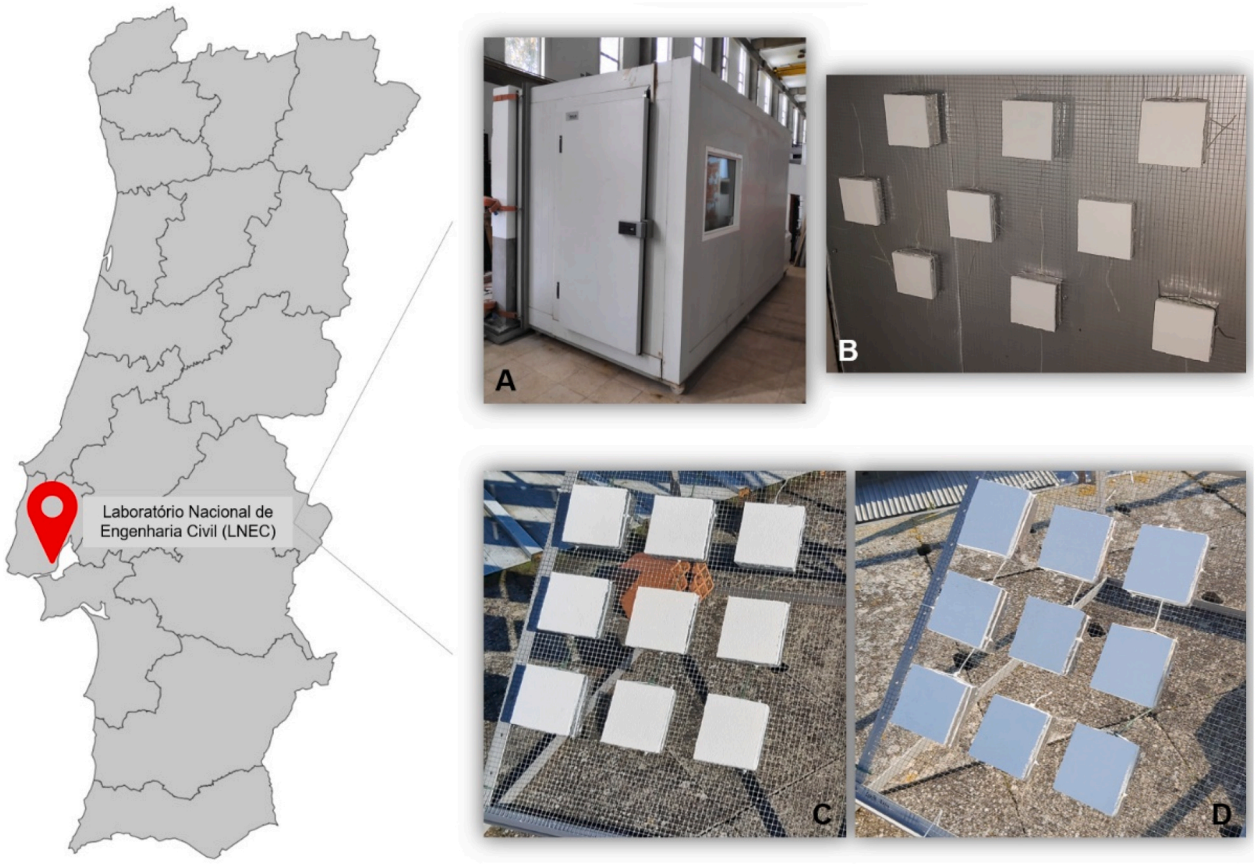

Fig. 3. Hygrothermal and natural aging tests: climatic chamber FitoClima 700EDTU (A); specimens fixed on a rack inside the climatic chamber (B); natural exposure of specimens facing South (C) and facing North (D).

the rendering system (base coat + finishing coat) at a dept of immersion of approximately 3 mm (Fig. 5A). The mass variation of the specimens caused by water absorption was then monitored at given time intervals (3 min, 1 h, 2 h, 4 h, 8 h, 24 h and 48 h) (Fig. 5B). Results were analyzed considering the capillary water absorption coefficient (A_w) and the absorption curves, showing the mass of absorbed water (kg/m^2) as a function of the square root of time (min$^{0.5}$). The capillary water absorption coefficient represents the initial rate of absorbed water and is obtained according to Eq. (4), in which M_1 and M_2 represent respectively the specimens' mass (kg) at the beginning of the test and after 3 min and A is the immersed area (m^2).

$$A_w = \frac{M_2 - M_1}{A \times \sqrt{3}} \quad (4)$$

The drying kinetics was determined in the same conditioned room (T = 23 ± 2 °C; RH = 65 ± 5%) according to EN 16322 [27], with the test starting immediately after the capillary water absorption. The mass variation of the specimens due to water loss was monitored at given time intervals till mass stabilization (<1% variation). Results were analyzed considering the drying rates (DR1 and DR2) and the drying curves. The first drying rate (DR1) is determined considering the negative slope of the initial linear section of the drying curve, expressing the mass loss (kg/m^2) as a function of time (h). On the other hand, the second drying rate (DR2) is obtained considering the negative slope of the linear section of the drying curve, expressing the mass loss (kg/m^2) as a function of the square root of time (h$^{0.5}$). DR1 and DR2 mainly correspond to liquid water transport and water vapor diffusion, respectively.

The capillary water absorption and the drying kinetics of the thermal mortars of each system (tested alone) were also evaluated. Samples of thermal mortars with dimensions of approximately 80 mm × 40 mm × 40 mm were collected from the unaged, artificially aged, and one-year naturally aged specimens. The tests were carried out following the procedures used for testing the complete system as described above. Results were evaluated considering the water absorption curves.

2.3.3. Water vapor permeability

The dry cup method was adopted to determine the water vapor permeability of cylindrical specimens (Ø ~ 70 mm) of the multilayer insulation systems in unaged conditions, after accelerated hygrothermal aging, and after one year of natural aging. The test was carried out in environmentally controlled conditions with a T = 23 ± 2 °C and a RH = 50 ± 5%, according to EN 1015–19 [28] and EAD 040083-00-0404 [26]. All specimens were previously stored in a conditioned room till mass stabilization and then sealed within a plastic recipient containing a desiccant (calcium chloride - $CaCl_2$) at the bottom. The specimens were sealed using scotch tape and paraffin wax, with an air gap of ~20 mm between the desiccant and the thermal mortar. The specimens were then placed in the test chamber, forcing the water vapor flux from the chamber environment (50 ± 5% RH) to the interior of the cup (~0% RH). The specimens' mass was monitored daily till stabilization (<1% variation). The water vapor diffusion resistance coefficient (μ) was obtained according to Eqs. (5) and (6).

$$\Lambda = \frac{m}{A \times \Delta_p} \quad (5)$$

$$\mu = \frac{1.94 \times 10^{-10}}{\Lambda \times e} \quad (6)$$

In Eqs. (2) and (3), Λ is the water vapor permeance, m is the slope of the linear correlation between mass variation and time, A is the specimens' area, Δ_p is the difference between the internal and external vapor pressure and e is the thickness of the specimen.

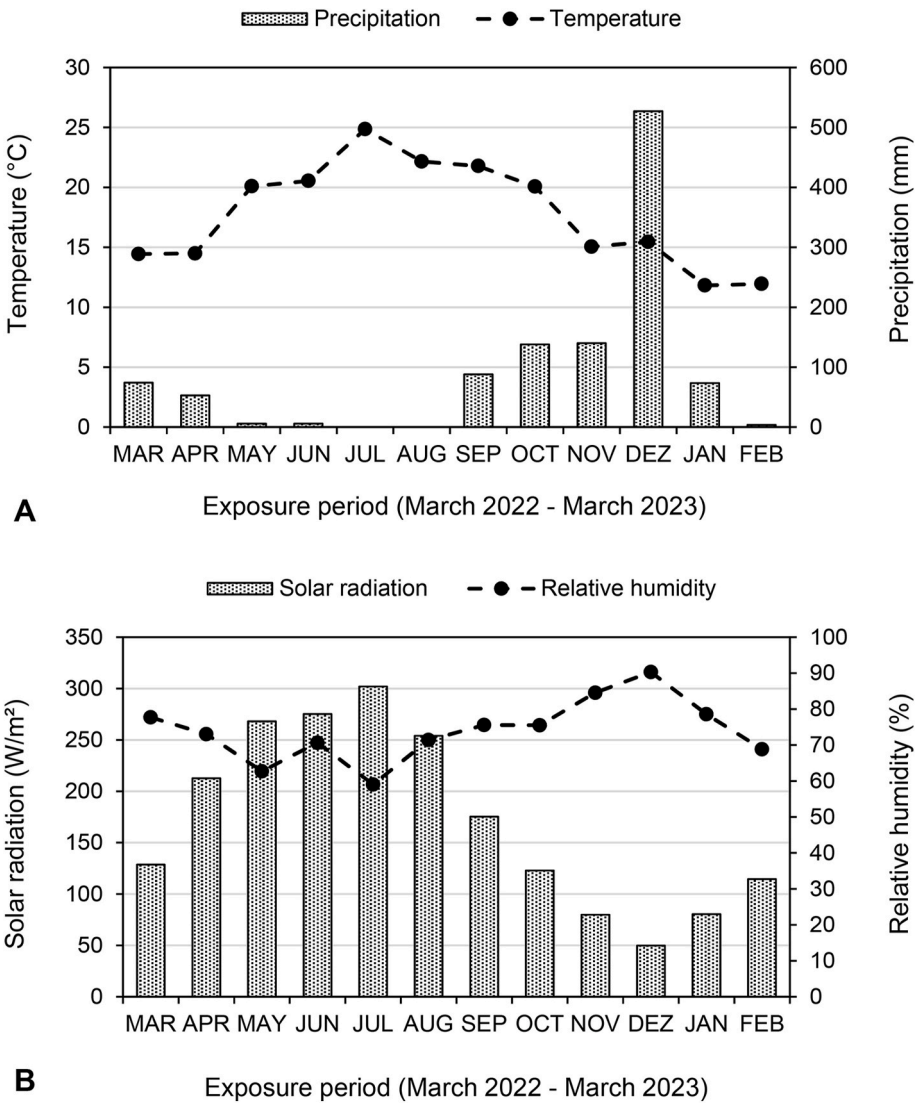

Fig. 4. Meteorological data registered during the exposure period: mean temperature and total precipitation (A); mean relative humidity and mean solar radiation (B).

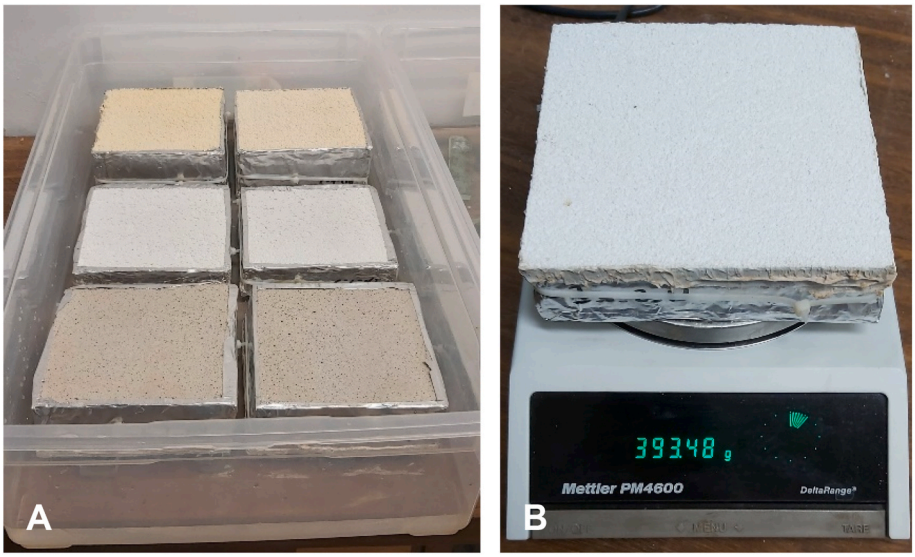

Fig. 5. Specimens during the capillary water absorption test (A) and monitoring of mass variation of one specimen after water absorption (B).

2.3.4. Gloss and color

Surface gloss was determined with a specular gloss meter Rhopoint Novo-Gloss Lite using a measurement geometry of 60°. All specimens were analyzed in nine different spots using a surface grid.

Color characterization tests were carried out with a Chroma Meter Minolta CR-410 determining the CIELAB coordinates (L^*, a^*, b^*), in which L^* ranges between 0 (black) and 100 (white) and represents the lightness, a^* ranges between -a^* (green) and +a^* (red) and represents the red/green coordinate, and b^* ranges between -b^* (blue) and +b^* (yellow) and represents the yellow/blue coordinate. All specimens were analyzed in nine different spots in specular component included mode (illuminant = D_{65}; observer angle = 2°; area of measurement (diameter) = 50 mm). The global color change (ΔE^*_{lab}) is obtained using Eq. (7) considering the reference colour (unaged condition) and the color of the specimens at each phase.

$$\Delta E^*_{lab} = \sqrt{(\Delta L^*)^2 + (\Delta a^*)^2 + (\Delta b^*)^2} \quad (7)$$

According to the study of Mokrzycki and Tatol [29], a value of global color change higher than 2 CIELAB units can be detected by an unexperienced observer.

2.3.5. SEM-EDS analysis

Scanning electron microscopy (SEM) analysis was performed using a SEM Thermoscientific Phenom ProX G6, working at an acceleration voltage of 20 kV. Prior to the SEM-EDS analysis, all samples were sputtered with an Au–Pd (80:20) film. This analysis was carried out only in coating samples collected from the unaged specimens, artificially aged specimens, and from those naturally aged after one year of exposure (facing North and South).

2.3.6. MIP analysis

To evaluate the microstructure of the unaged and aged thermal mortars, mercury intrusion porosimetry (MIP) was carried out using a Micromeritics AutoPore IV 9500, applying a maximum intrusion volume for low and high pressure of 1×10^5 mL g^{-1}. A surface tension of 485 × 10^{-3} N/m and a contact angle of the mercury with the samples of 140° were considered in the analysis.

2.3.7. Biological colonization

The susceptibility to biological colonization of the surface of the unaged and artificially aged specimens and thermal mortars was assessed using a method previously adapted and validated for ETICS by Parracha et al. [30]. Three unaged and artificially aged specimens of each system and corresponding thermal mortars with dimensions of ~50 mm × 50 mm × 20 mm were steam sterilised for 20 min in an autoclave and then placed on test flasks with culture media (4% malt and 2% agar concentration). Afterwards, a 2 mL volume of a spore suspension of *Aspergillus niger* and *Penicillium funiculosum* (artificial inocula) was uniformly applied on the specimens and surrounding culture media. The test flasks were placed for four weeks in a culturing chamber at T = 22 ± 1 °C and 70 ± 5% RH. Biological colonization was visually assessed each week using the scale of Table 4 [31]. A second group of unaged and artificially aged specimens (natural inocula) was exposed in the same conditions but without any sterilization or inoculation. A control group with six wood samples (*Pinus pinaster*) was used to validate the test results (i.e., three samples for the artificial inocula and other three for the natural inocula). After four weeks, all specimens and controls were cautiously removed from the test flasks, and the final percentage of contaminated surface evaluated with a stereo microscope Olympus SZH10 (Olympus SC30 image acquisition system and Olympus LabSens software).

Table 4
Scale for biological colonization assessment defined in ASTM D5590-17 [31].

Rating	Contaminated area [%]	Description
0	0	None
1	<10	Traces of growth
2	10 to 30	Light growth
3	30 to 60	Moderate growth
4	>60	Heavy growth

The presence of biological colonization was visually assessed on the surface of the naturally aged specimens after 3, 6, 9 and 12 months of exposure. The percentage of contaminated surface was evaluated by the same experienced observer using the stereo microscope Olympus SZH10 as described above.

2.3.8. Statistical analysis

Differences between aging conditions (i.e., unaged, artificially aged, naturally aged facing North and facing South) were evaluated through analysis of variance (ANOVA), followed by the Tukey test (p-value <0.05). The analysis was carried out with the SPSS Statistics V26 software from IBM.

3. Results

3.1. Visual and stereomicroscope observations

Stereomicroscope observations carried out after hygrothermal accelerated aging confirmed the presence of vast microcracking and occasional material loss on the surface of the multilayer insulation systems, especially in the case of S2 (Fig. 6A), that was finished with an acrylic-based FC with siloxane resin and composed of a TM with mixed binders and EPS aggregates (Table 1). Indeed, the occurrence of surface microcracking can be explained by surface embrittlement caused by aging and hygric stresses occurring during the accelerated aging procedure due to the significant temperature variation (see Table 3) [32,33]. Moreover, the surfaces of the systems seemed to be whiter and slightly smoother after artificial aging (e.g., Fig. 6A).

When considering the naturally aged systems, surface condensation was visually detected on all specimens since the beginning of the exposure, especially in the early morning and in systems facing North. Moreover, extensive surface microcracking was also observed in the naturally aged systems just after 3 months of outdoor exposure. In fact, microcracking was slightly higher in the systems oriented towards North and especially relevant in the case of system S2 (Fig. 6B), in accordance with similar observations of the artificially aged specimens. It is important to note that microcracking favors surface water retention, potentiating the occurrence of further anomalies (e.g., biological colonization) [34,35]. Additionally, some dirt deposition was also observed on the surfaces of the naturally aged systems facing both North and South, thus promoting aesthetic alteration (Fig. 6C).

3.2. Water transport properties

The capillary water absorption curves of the unaged, artificially, and naturally aged systems are shown in Fig. 7. The lowest capillary absorption values were always obtained for the unaged specimens, regardless of the tested system. In fact, all systems presented a capillary water absorption after 1 h lower than 1 kg/m^2, respecting the threshold defined in the EAD 040083-00-0404 [26] for ETICS. Moreover, the long-term capillary absorption (i.e., at the end of the test) of the unaged systems was lower than 1.5 kg/m^2, showing a decrease in the water absorption rate after the first hour of test. The level of capillary water absorption at the end of the test assumed values between 0.79 kg/m^2 for S2 and 1.40 kg/m^2 for S3 (Fig. 7). After hygrothermal accelerated aging, the values of absorbed water significantly increased when compared to the unaged systems. The highest increase (+967%) of capillary absorption at the end of test was obtained for the non-commercialized system S3 (acrylic-based FC and TM with mixed binders and silica aerogel), whereas the lowest (+270%) was obtained for system S1 (acrylic-based FC and TM with lime and EPS aggregates). In this case, the

Fig. 6. Microcracking observed on the surface of the artificially aged (A) and 3-months naturally aged system S2 (B); dirt deposition on the surface of the naturally aged system S3 after 9 months of outdoor exposure facing North (C).

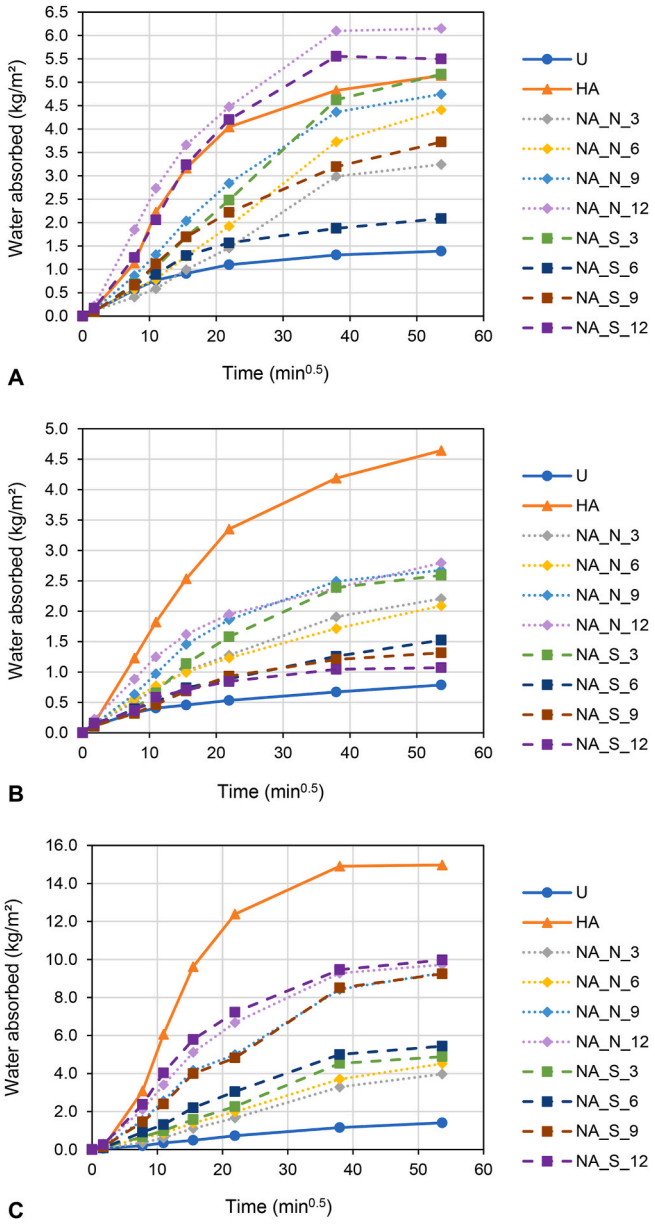

Fig. 7. Capillary water absorption curves of unaged (U), artificially (HA) and naturally (NA) aged systems S1 (A), S2 (B) and S3 (C).

water absorption rate started decreasing only after 4 h of test (Fig. 7). These results revealed that after accelerated artificial aging the acrylic-based finishing coat is no longer capable of effectively protecting the aged system against liquid water penetration. Furthermore, results also showed that capillary water absorption is significantly higher in the thermal mortars collected from the aged systems in comparison with the unaged mortars, indicating that accelerated aging affected not only the performance of the multilayer rendering system, but also that of the thermal insulating mortar (Fig. 8). In this case, the highest capillary absorption increase (+672%) was obtained for TM3, the mortar with mixed binders and silica aerogel and the lowest (+30%) for TM1, the mortar with lime and EPS aggregates.

Concerning the naturally aged specimens, results revealed different trends for the three multilayer insulation systems. Naturally aged system S2 (acrylic-based FC with siloxane resin and TM with mixed binders and EPS aggregates) showed the best performance (i.e., lowest capillary water absorption) after one year of outdoor exposure (Fig. 7B). Interestingly, results showed a slight decrease of capillary absorption for longer exposure time in the case of S2 specimens facing South. These results are in accordance with the decrease of capillary water absorption also observed for the naturally aged TM2 mortar (collected from the system S2 facing South) when compared to the unaged mortar (Fig. 8B). On the other hand, the water absorption of S2 specimens facing North increased with exposure time, with the highest capillary absorption registered after one year of exposure (~2.8 kg/m^2). Therefore, naturally aged system S2 obtained values of capillary absorption at the end of the test ranging between 1 kg/m^2 and 2.8 kg/m^2. These values are lower than those obtained after artificial aging (~4.6 kg/m^2), but higher than those of unaged S2 specimens (~0.8 kg/m^2).

In the case of system S1 (acrylic-based FC and TM with lime and EPS aggregates), results showed an increase of capillary water absorption with exposure time for specimens oriented towards North, reaching ~ 6.1 kg/m^2 of absorbed water (at the end of the test) after one year of exposure and surpassing the value obtained for the artificially aged system (~5.1 kg/m^2). With the exception of the absorption value registered after 3 months of exposure, a similar trend was observed for the specimens facing South (i.e., capillary absorption increases with exposure time). Nevertheless, S1 specimens oriented towards South absorbed less water than those facing North, regardless of the exposure time (i.e., 6-, 9- or 12-months exposure). In summary, naturally aged S1 obtained capillary water absorption values at the end of the test in the range between 2 kg/m^2 and 6.1 kg/m^2, which is 50%–342% higher than the result obtained for the unaged system (1.39 kg/m^2).

For the acrylic-based system with cement-based BC and TM with mixed binders and silica aerogel (S3), an increase of capillary water absorption with exposure time was observed, especially after 6 months of outdoor exposure in specimens facing both North and South (Fig. 7C). In fact, results were slightly higher for specimens oriented towards South considering similar exposure time. In this case, after 3–6 months of natural aging, results suggested a capillary absorption at the end of

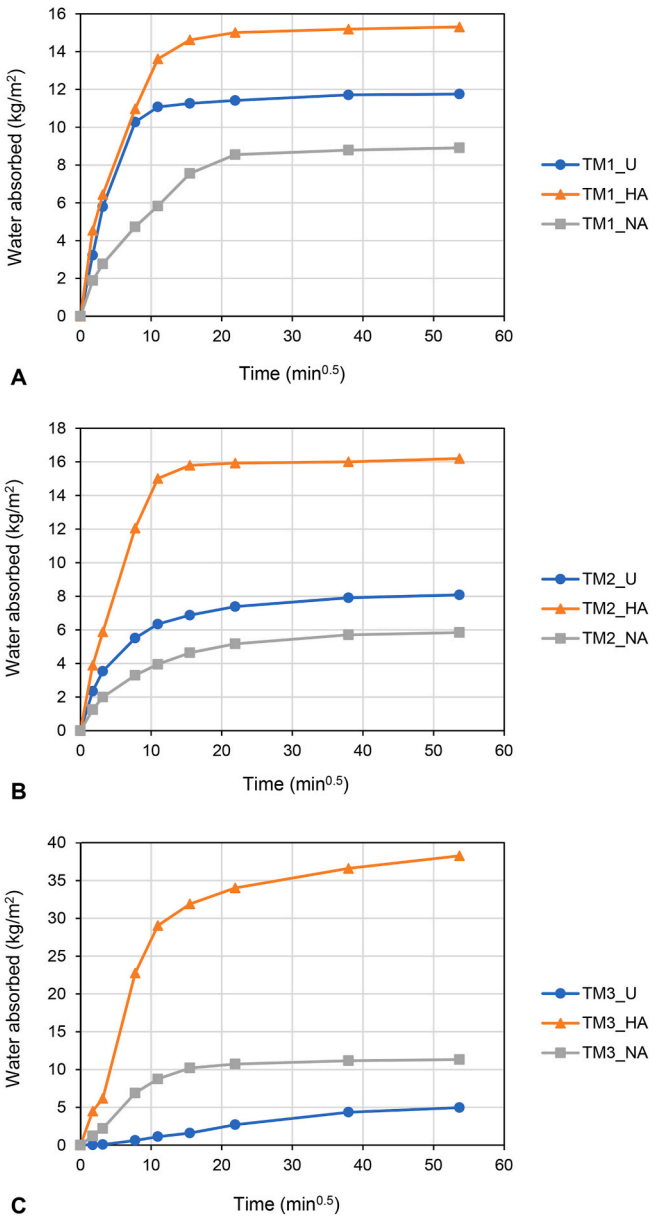

Fig. 8. Capillary water absorption curves of unaged (U), artificially (HA) and naturally (NA) aged thermal mortars TM1 (A), TM2 (B) and TM3 (C) collected from the multilayer insulation systems.

the test ranging between ~3.9 kg/m^2 and ~5.4 kg/m^2 (i.e., 183%–288% higher in comparison to unaged conditions). A significant water absorption increase is then obtained when considering the results after 9 and 12 months of exposure, with values above 9 kg/m^2 (Fig. 7C). However, the results were still lower than those obtained after artificial aging. It is worth noting that, after artificial and natural aging, the capillary water absorption of the aerogel mortar tested alone (TM3) significantly increases when compared to the unaged mortar, reaching values up to 35 kg/m^2 of absorbed water after accelerated aging (Fig. 8C).

Fig. 9 shows the results of the capillary water absorption coefficients (A_w) obtained for the unaged, artificially and naturally aged systems. These results represent the initial rate of absorbed water (i.e., in the first 3 min of test) with the objective mainly of evaluating the water performance of the rendering system. When considering unaged conditions, the lowest A_w is obtained for the acrylic-based system S3, with rather similar results in the case of unaged systems S1 and S2. After

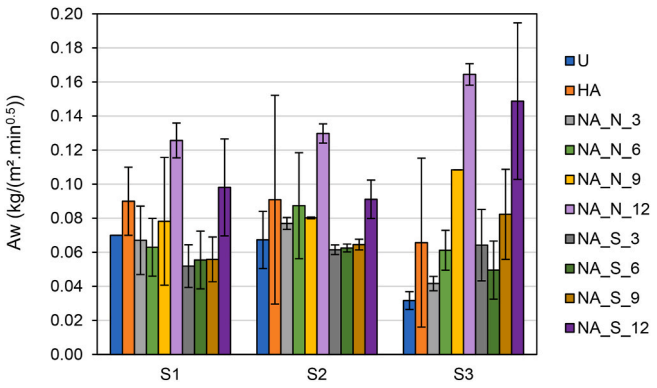

Fig. 9. Capillary water absorption coefficient of unaged (U), artificially (HA) and naturally (NA) aged systems (average values and relative standard deviation).

hygrothermal accelerated aging, A_w results were slightly higher for the three systems, with a broad range of standard deviation values indicating a less consistent water performance. Finally, similar trends were obtained for the three naturally aged systems, with the results generally showing greater A_w values in specimens facing North. With exception of system S3 oriented towards North, it can be observed that results are not significantly different after 3-, 6- or 9-months exposure, regardless of the systems' orientation. Nonetheless, a significant A_w increase was obtained after one year of natural aging in both systems facing North and South, possibly indicating a degradation of the finishing coat after one year of natural exposure.

Fig. 10 and Table 5 show, respectively, the drying curves and the drying rates obtained for the unaged, artificially and naturally aged systems. The lowest values of DR1 and DR2 (i.e., a slower drying process) were generally obtained for the unaged systems, with all specimens achieving mass stabilization after 17 days (S1), 7 days (S2), and 12 days (S3) of drying. On the other hand, the artificially aged systems obtained the highest DR1 (i.e., high liquid water transport to the surface) and DR2 (i.e., high water vapor transport to the surface). In this case, mass stabilization was achieved after 17 days (S1), 20 days (S2) and 65 days (S3) of drying.

Interestingly, the drying process of the acrylic-based system S1 was considerably faster after artificial aging, with unaged and artificially aged specimens achieving the same time for mass stabilization (17 days), despite the considerably higher amount of absorbed water observed after artificial aging (Fig. 7A). However, the same trend was not verified after natural aging, with these specimens obtaining greater capillary water absorption and a slower drying process when compared to the artificially aged specimens. As visualized in Fig. 11A, this behavior is not related to the drying kinetics of the naturally aged EPS thermal mortar, but rather with the alteration of the drying kinetics of the rendering system. Mass stabilization was achieved after 69 days and 57 days of drying for the naturally aged system S1 facing North and South, respectively.

When considering the drying results obtained for the acrylic-based system S2 with an EPS thermal mortar, it can be observed that a significant alteration in the drying process is only detected after artificial aging, with the naturally aged specimens presenting a drying behavior similar to that obtained in unaged conditions (Fig. 10B and Table 5). It is interesting to note that a similar trend was observed looking at the drying kinetics of the unaged and aged TM2 (Fig. 11B) (i.e., a faster drying process for the artificially aged mortar, and no significant alteration in the drying kinetics of the naturally aged TM2 when compared to unaged conditions).

On the other hand, results showed significantly higher values of DR2 (i.e., high water vapor transport to the surface) for the non-commercialized system S3 after artificial and natural aging (+433%

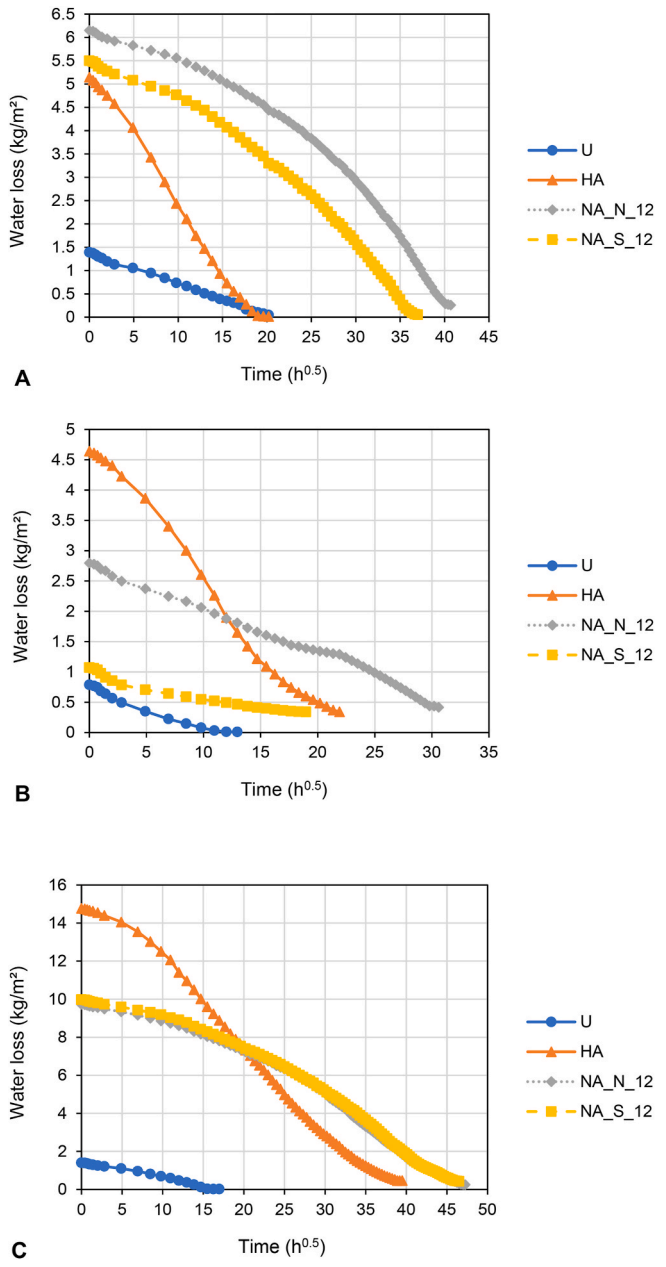

Fig. 10. Drying curves of unaged (U), artificially (HA) and naturally (NA) aged systems S1 (A), S2 (B) and S3 (C).

and +162%, respectively). Nevertheless, a significant increase of DR1 (i.e., high liquid water transport to the surface) in the case of S3 was only detected after artificial aging (Table 5).

Results of the water vapor diffusion resistance coefficient (μ) obtained for the unaged, artificially and naturally aged systems are shown in Fig. 12. The highest μ-value in unaged conditions was obtained for the acrylic-based system S1 with an EPS thermal mortar, whereas the lowest was achieved for the acrylic-based system S3 with an aerogel thermal mortar. In fact, results showed that multilayer insulation systems are significantly less water vapor permeable than the thermal mortars. Considering the unaged thermal mortars with EPS aggregates, the highest value (μ = 8) was obtained for TM1 and the lowest (μ = 6) for TM2. The aerogel mortar presented higher water vapor permeability (μ = 5). Results are in accordance with previous studies evaluating the water vapor permeability of mortars with EPS aggregates (e.g., Ref. [10]) or silica aerogel (e.g., Ref. [17]).

After artificial and one year of natural aging, the water vapor permeability of the acrylic-based system S1 was significantly lower (Fig. 12), most probably due to a modification of the pore size distribution of the rendering system [22,46]. A similar trend was also observed for the acrylic-based system S3, with an aerogel thermal mortar (Fig. 12). However, a significantly lower μ-value (i.e., higher water vapor permeability) in the case of the acrylic-based system S2 was only achieved after artificial aging, in accordance with the drying kinetics results (Table 5). This leads to a decrease of water accumulation within the system only in the artificially aged specimens, as well as a decrease in the risk of internal water condensation [47,48]. Conversely, the naturally aged S2 specimens absorbed significantly more water (Fig. 7B) without a significant alteration in the drying process (Fig. 10B and Table 5).

3.3. Gloss and color

Fig. 13 shows the results of the surface gloss of the unaged, artificially, and naturally aged systems. A significant gloss decrease ($p < 0.05$) was obtained for the systems after accelerated artificial aging, most probably due to the heat/rain cycles facilitating surface washing. Moreover, significantly lower gloss values were obtained after only 3 months of natural aging considering the specimens oriented towards North ($p < 0.05$). In fact, for the naturally aged specimens facing South, surface gloss decrease was only statistically significant different after 6 months of outdoor exposure, thus indicating that aesthetic alteration can be more pronounced in the specimens oriented towards North at an early stage (Fig. 13). Nevertheless, gloss variation was not significantly different among exposure conditions (i.e., North and South) after 6 months of outdoor exposure.

The highest gloss variation after artificial aging was obtained for S2 (acrylic-based with siloxane resin FC) and the lowest for S3 (acrylic-based with mineral aggregates FC). In the case of S2, results showed that comparable gloss variation between artificially and naturally aged specimens was obtained in the period between 3 and 6 months of outdoor exposure (Fig. 14). On the other hand, a much shorter period of time should be considered to compare surface gloss of aged system S1, i.e., ~3 months and between 3 and 6 months considering S1 specimens facing North and South, respectively. For S3, results showed a similar gloss variation between the artificially and the naturally aged system in the period between 0 and 3 months considering specimens facing North and after 3 months of exposure in the case of those facing South (Fig. 14).

The average results of the colorimetric coordinates (L*, a*, b*) of the unaged, artificially, and naturally aged systems are shown in Fig. 15. The lightness values (L*) obtained after hygrothermal accelerated aging were not significantly different ($p = 0.999$) from those registered in unaged conditions (i.e., unaged specimens). However, lightness results were significantly lower ($p < 0.01$) after 3 months of natural aging,

Table 5
Drying rates (DR1 and DR2) of unaged, artificially, and naturally aged systems.

System (S)	DR1 [kg/(m².h)]				DR2 [kg/(m².h^0.5)]			
	U	HA	NA_N_12	NA_S_12	U	HA	NA_N_12	NA_S_12
S1	0.032	0.045	0.028	0.036	0.065	0.295	0.157	0.178
S2	0.037	0.052	0.037	0.036	0.069	0.248	0.071	0.032
S3	0.023	0.047	0.029	0.029	0.087	0.464	0.228	0.227

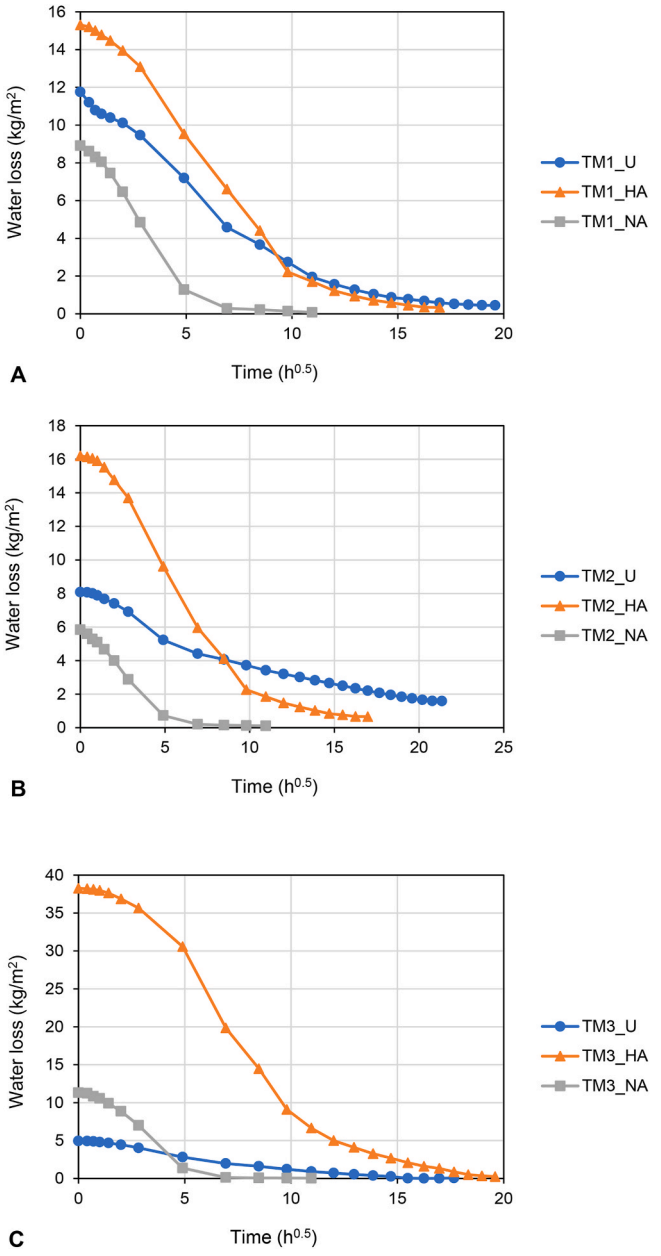

Fig. 11. Drying curves of unaged (U), artificially (HA) and naturally (NA) aged thermal mortars TM1 (A), TM2 (B) and TM3 (C) collected from the multilayer insulation systems.

regardless of the exposure orientation (North or South). Moreover, naturally aged systems facing North become significantly darker (i.e., lower L*), when compared to systems oriented towards South ($p < 0.05$). In fact, both systems facing North and South presented a considerably darker tone after 3, 6 and 9 months of outdoor exposure, followed by a lightness stabilization after 9 months of natural aging.

As expected, the chromatic coordinate a* was not significantly affected after hygrothermal accelerated aging ($p = 0.842$), with the highest values obtained for the acrylic-based with siloxane resin system S2 (Fig. 15B). After 3 months of outdoor exposure, the systems facing South acquired a significantly more reddish tone when compared to systems facing North. Nevertheless, the highest a* increase was registered after 6 months of exposure, due to a significant accumulation of dust in the surface of the systems caused by a Sahara dust storm affecting Portugal in the end of June 2022 (i.e., approximately 4 months after the beginning of the natural exposure). Additionally, a slight increase of a*

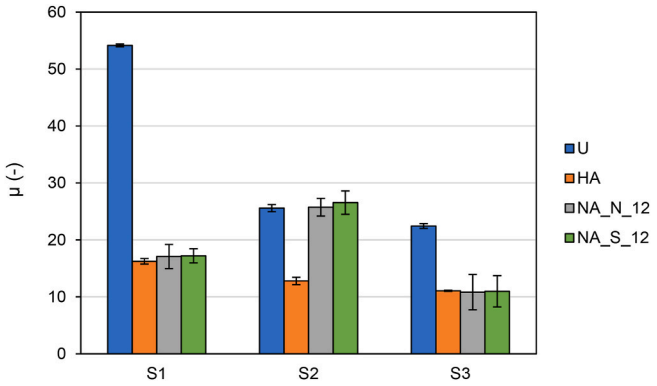

Fig. 12. Water vapor diffusion resistance coefficient (μ-value) of unaged (U), artificially (HA) and one-year naturally (NA) aged systems (average values and relative standard deviation).

was obtained after 9 months of exposure, with no significant differences registered between specimens facing North and South ($p < 0.05$). After 12 months of exposure, a* values were not significantly different from those obtained after 9 months. In some cases, there was a slight increase of a* (e.g., S1 facing South), in the vast majority a slight a* decrease was registered. This result may be explained by the significant amount of rainfall registered in December in Lisbon (Fig. 4A), facilitating surface washing.

Furthermore, the chromatic coordinate b* was not significantly affected after accelerated aging ($p = 0.814$), with the highest increase obtained for system S2 (i.e., a slightly higher yellowish tone) (Fig. 15C). On the other hand, a significantly higher yellowish coloration was detected after 3 months of outdoor exposure in systems facing both North and South ($p < 0.01$). Moreover, systems become considerably more yellowish after 6 months of natural aging, regardless of the exposure orientation (North or South). A stabilization of the yellow tone was then observed after 6 months of aging, without significant differences detected from there till one year of exposure.

Finally, a global color change (ΔE^*_{lab}) lower than 2 CIELAB units was obtained in the case of the artificially aged systems (Fig. 16), meaning that all aesthetic alteration caused by the accelerated aging procedure cannot be detected by an unexperienced observer [29]. When considering the naturally aged specimens, the threshold value of 2 CIELAB units was achieved before the 3 months of outdoor exposure for specimens facing both North and South, reaching values up to 10 CIELAB units after one year of aging. In fact, results are in accordance with the visual analysis (i.e., aesthetic alteration was detected even before the 3 months of natural aging with the deposition of particulate matter on the surface of systems). It is interesting to note that a positive variation of the overall color change was observed from the beginning till 9 months of aging, followed by a negative variation for some systems after one year of exposure. As previously stated, this can be due to surface washing caused by the significant amount of rainfall in December 2022 (Fig. 4A).

3.4. SEM-EDS analysis

SEM microphotographs of the unaged, artificially, and one-year naturally aged surfaces of the systems are shown in Fig. 17. Results showed a dense and compact structure in the case of the unaged system S1 (Fig. 15A), with some micro lacunae, material loss and microcracking observed after artificial aging (Fig. 17B). After one year of natural aging, it can be observed a slight increase of surface roughness with a more heterogeneous surface and deposition of dust. These data can justify the significantly higher capillary water absorption of the artificially and naturally aged specimens when compared to the unaged S1 (Fig. 6A). Moreover, SEM-EDS results also showed the presence of biological

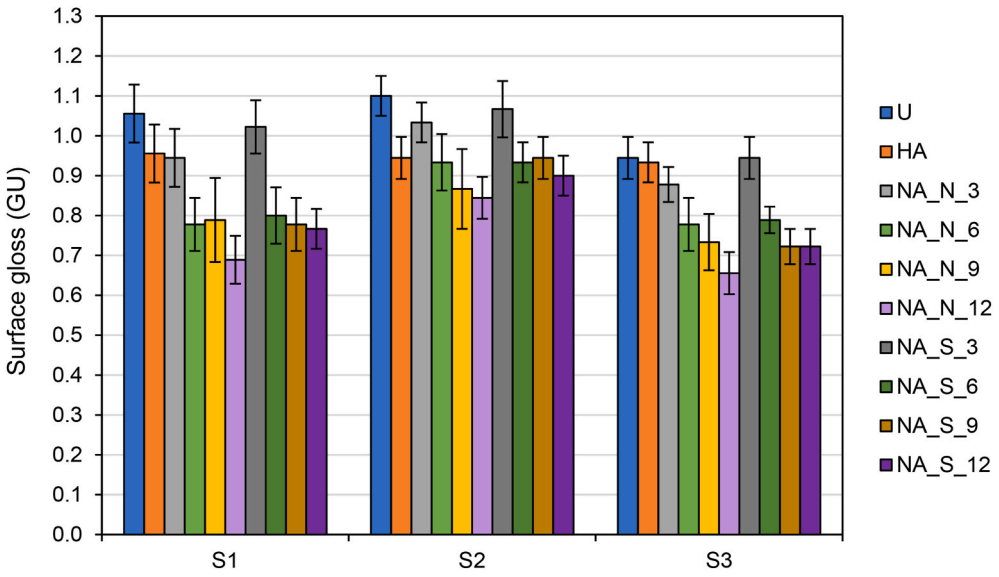

Fig. 13. Specular gloss of unaged (U), artificially (HA) and naturally (NA) aged systems (average values and relative standard deviation).

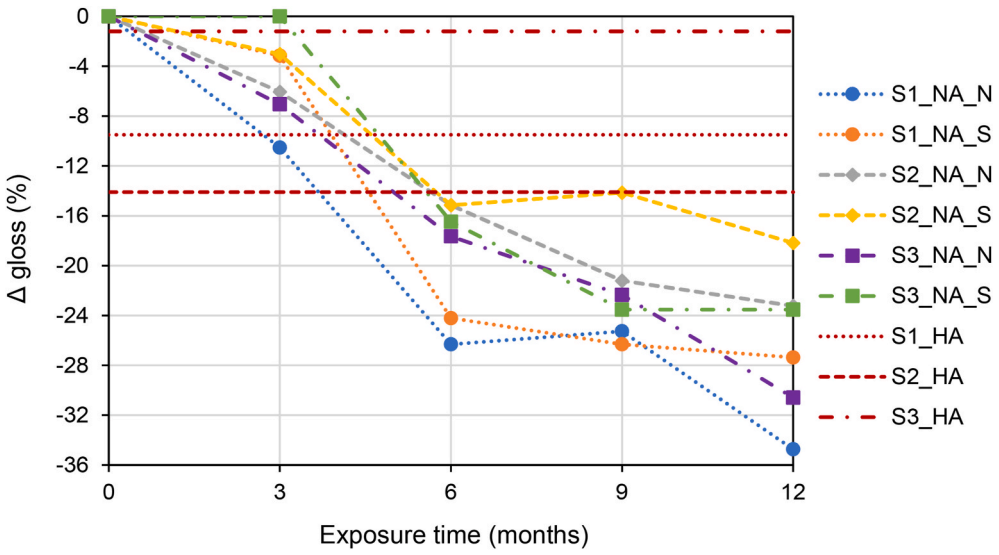

Fig. 14. Specular gloss variation after artificial (HA) and natural (NA) aging.

colonization in the surface of the naturally aged system S1 (Fig. 17C), with the EDS spectrum indicating considerable amounts of calcium (Ca), titanium (Ti) and silica (Si) (Fig. 17D). The significant percentages of Ca, Ti and Si detected in the surface of the acrylic-based system S1 can be respectively attributed to the addition of calcium carbonate ($CaCO_3$) (used as filler and pigment), titanium dioxide (TiO_2) (used as photocatalytic additive and pigment) and the siliceous aggregate (frequently used in the FC formulation to increase surface roughness and durability) [36,37].

System S2 presented a homogeneous and compact structure before aging (Fig. 17E). After accelerated aging, SEM microphotographs showed a significant degradation of the finishing coat with a loss of the binding capacity of the siloxane resin (Fig. 17F), thus leading to the disintegration of the coating and resulting in the formation of surface voids and extensive microcracking (see Section 3.1). The naturally aged S2 specimens showed a less compact structure with micro-abrasion of the superficial patina in some spots inducing an angular morphology of the particles and slightly increasing surface roughness (Fig. 17G). The presence of Ca and Ti was also detected in this system (Fig. 17H). In fact, the addition of TiO_2 in the formulation of the finishing coat can provide self-cleaning properties and a biocide effect to the system [38,39].

Furthermore, the system finished with an acrylic-based with mineral aggregates FC (i.e., S3) presented a dense and compact structure before aging (Fig. 17I), which was similar to the structure observed in the unaged acrylic-based system S1 (Fig. 17A). Both artificially and naturally aged specimens presented extensive microcracking and material loss with smoother surfaces when compared to the unaged specimens (Fig. 17J). Further magnification showed the presence of occasional biological colonization in the artificially aged specimens (Fig. 17K). In fact, system S3 presented a significant increase of capillary water absorption after aging (Fig. 6C) showing that the coating is no longer effective enough to protect the thermal mortar against weathering. This result can possibly be explained by a lack of compatibility between the rendering system and the thermal mortar. Moreover, the significant amount of absorbed water during the hygrothermal cycles together with the formation of extensive microcracking may have favored biological growth in the surface of the systems [40,41].

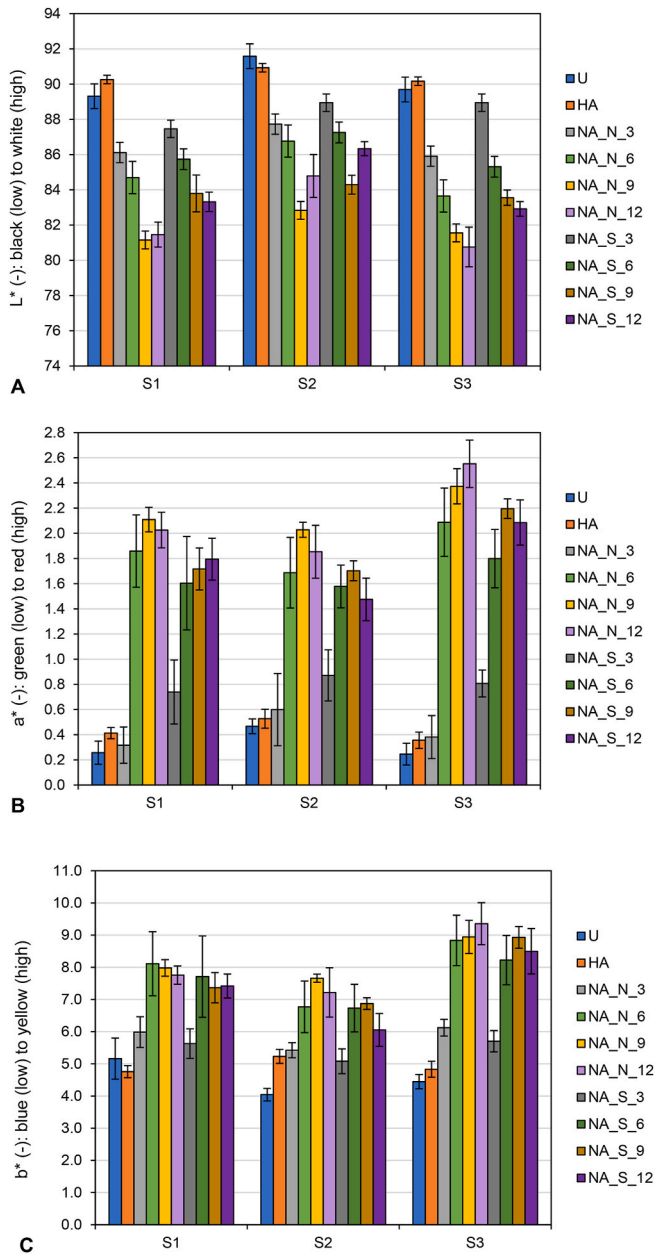

Fig. 15. Results of colorimetric coordinates L* (A), a* (B) and b* (C) of unaged (U), artificially (HA) and naturally (NA) aged systems (average values and relative standard deviation).

3.5. MIP analysis

Mercury intrusion porosimetry (MIP) analysis was carried out to evaluate the microstructure of the unaged, artificially, and naturally aged thermal mortars. Fig. 18 and Table 6 show the pore size distribution curves and some porosity characteristics of the mortars, respectively.

Unaged and aged thermal mortars TM1 and TM2, with EPS as lightweight aggregates, presented a similar unimodal distribution with a large number of pores in the range between 5 μm and 10 μm (Fig. 18A and 17B). In fact, the total porosity of both mortars slightly decreased after artificial and natural aging (Table 6), whereas the median pore diameter and the total pore area increased after aging, with the highest results obtained after hygrothermal accelerated aging (Table 6). On the other hand, unaged and aged aerogel mortar TM3 showed a bimodal distribution, which was more pronounced after aging (Fig. 18C). In fact,

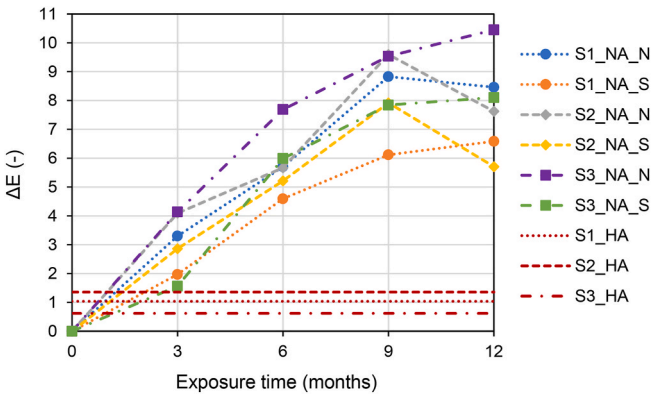

Fig. 16. Average values of global color variation of artificially (HA) and naturally (NA) aged systems. (For interpretation of the references to color in this figure legend, the reader is referred to the Web version of this article.)

two significant peaks can be identified in the distribution curves: the first corresponding to a major concentration of pores with a diameter in the range between 5 μm and 10 μm; the other related with a wider range of pores between 10 μm and 100 μm. This latter peak significantly increased after accelerated aging, with the mean pore diameter (vol.) reaching 7.714 μm (Table 6). Therefore, it can be noted that the alteration of the pore structure of TM3 observed after accelerated and natural aging is mainly related to the variation detected in the pore diameter range between 10 μm and 100 μm (Fig. 18C). Moreover, an increase of the total porosity of the aerogel mortar was registered after accelerated (~95%) and natural (~93%) aging, when compared to the mortar in unaged conditions (~89%) (Table 6).

3.6. Biological colonization

Table 7 presents the average results of mold development on the surface of the artificially aged multilayer insulation systems. When analyzing the results obtained with the natural inocula, traces of mold growth (<10% of contaminated area) were observed in the three tested systems only after four weeks of incubation. On the other hand, the results obtained with the artificial inocula showed slightly higher mold development, with traces of growth detected earlier in the test (i.e., after 2 and 3 weeks of incubation) (Fig. 19A). The highest rate of mold growth was observed for the acrylic-based with mineral aggregates system S1, in accordance with the results obtained with the natural inocula (Fig. 19B). All controls were rated as 4 at the end of the test (>60% of contaminated area), thus allowing to validate the test results.

When considering the average results of mold development obtained for the thermal mortars (Table 8), considerable mold growth was detected for the artificially aged aerogel mortar after four weeks of incubation. In fact, the rate of mold development was significantly higher in the artificially aged aerogel mortar (Fig. 20B) when compared to unaged specimens (Fig. 20C), regardless of the type of inocula (artificial or natural). This result can be explained by the significantly higher capillary water absorption of the aerogel mortar after accelerated aging (see Section 3.2; Fig. 8C), facilitating water retention and increasing the risk of biological colonization [40]. The results obtained for the EPS thermal mortars (i.e., TM1 and TM2) were considerably lower and not significantly different among each other, either considering the aging condition or the type of inocula (Fig. 20A and D). In fact, the average results of mold development obtained for the thermal mortars were lower than those gathered for expanded cork (ICB) samples and similar to those registered for mineral wool (MW) samples [30,42]. Nonetheless, mold development observed on the unaged and aged thermal mortars was higher than that of expanded polystyrene (EPS) boards [43]. It can thus be concluded that an enhanced performance of the rendering system is essential to avoid biological colonization on the

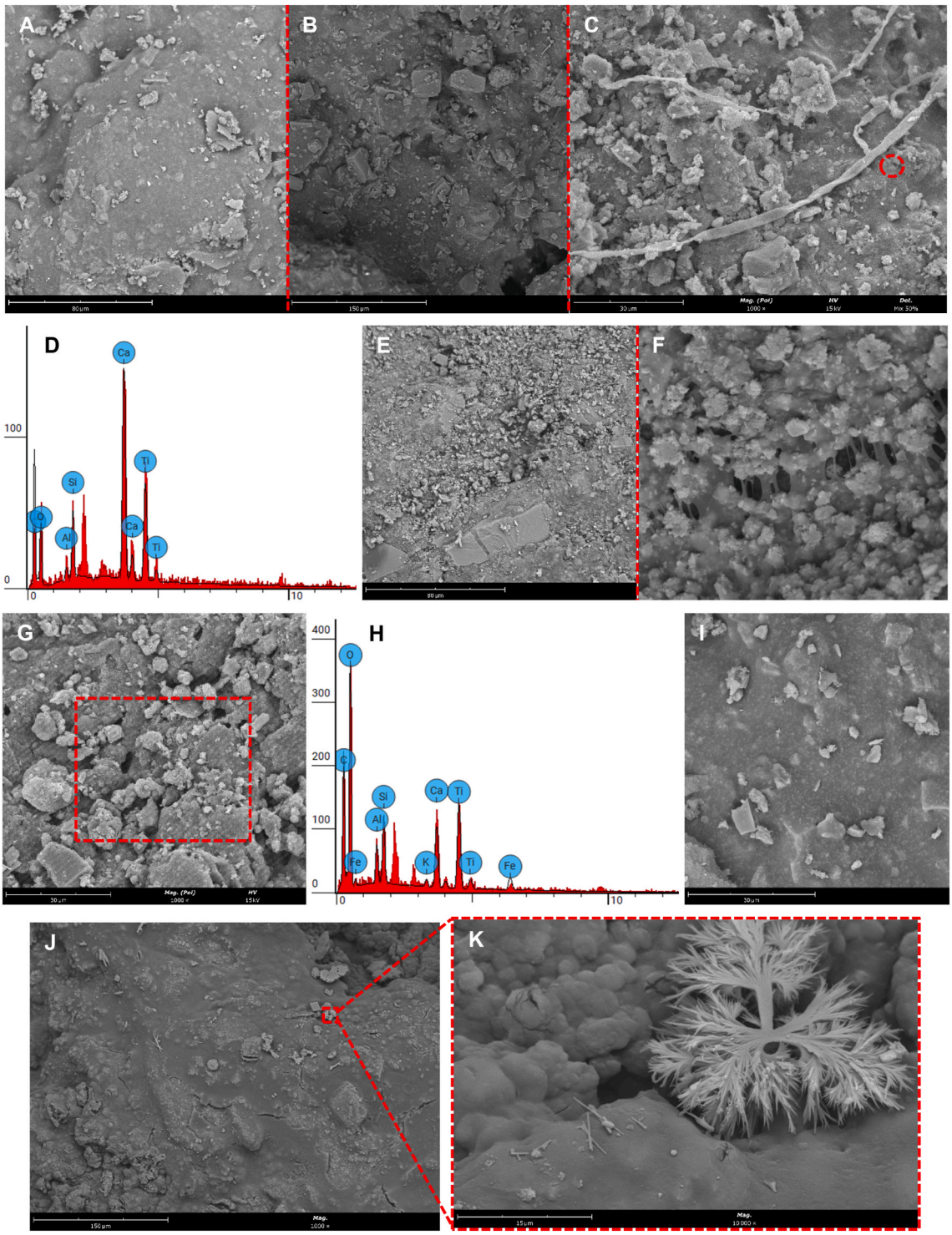

Fig. 17. SEM microphotographs of system S1: unaged (A), after artificial aging (B), and after one year of natural aging facing North (C), and EDS spectrum (D) of the area marked in red in (C); system S2: unaged (E), after artificial ageing (F), and after one year of natural aging facing South (G), and EDS spectrum (H) of the area marked in red in (G); system S3: unaged (I), and after artificial aging (J), with (K) showing the presence of biological colonization in the surface of the aged system. (For interpretation of the references to color in this figure legend, the reader is referred to the Web version of this article.)

thermal mortar and therefore in the complete multilayer insulation system.

Biological colonization results on the surface of the naturally aged systems are presented in Table 9. Mold development was higher in all specimens facing North, showing traces of growth (<10% of contaminated area) after 6 months of outdoor exposure. Considering the specimens oriented towards South, biological growth was only detected after 9 months of natural aging, with only one out of three specimens of each system rated as 1 (i.e., traces of growth), due to occasional hypha grow on its surface. Conversely, the highest mold development after one year of aging was observed for the acrylic-based system S1, most probably due to the increase of surface roughness, water retention and deposition of dust observed in the naturally aged system (see Sections 3.2 and 3.4) [44,45].

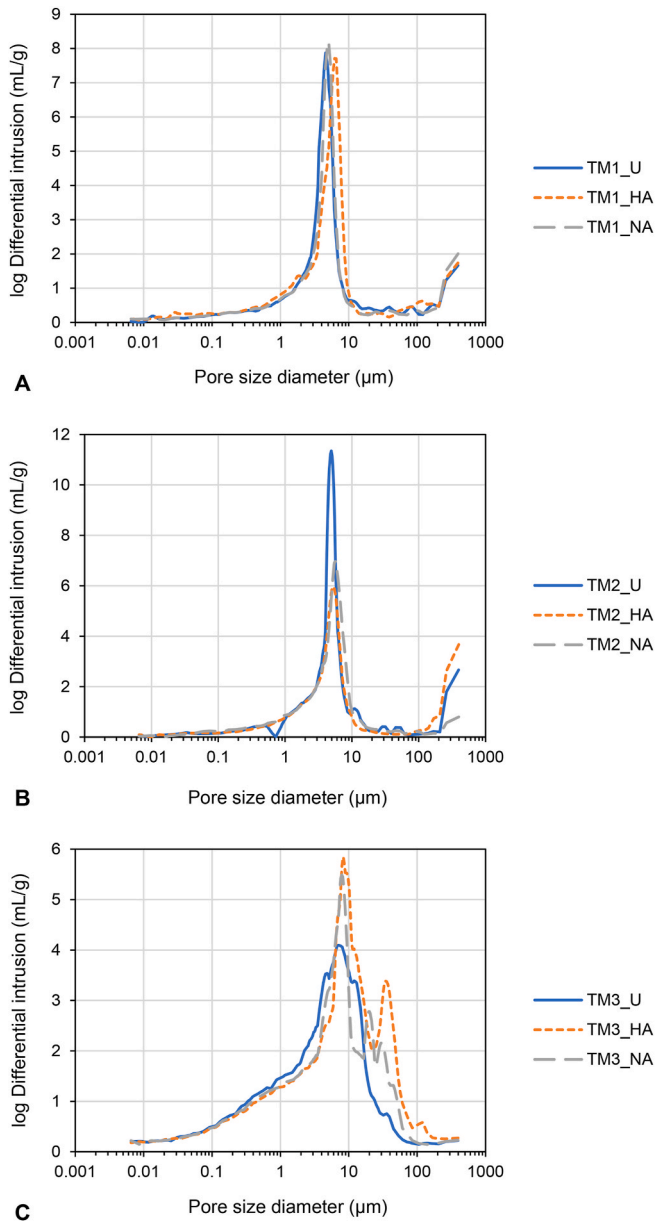

Fig. 18. Pore size distribution curves of unaged (U), artificially (HA) and naturally (NA) aged thermal mortars TM1 (A), TM2 (B) and TM3 (C) collected from the multilayer insulation systems.

Table 6
Porosity characteristics of the unaged and aged thermal mortars.

Thermal mortar (TM)	Aging condition	Porosity [%]	Median pore diameter (vol.) [μm]	Total pore area [m^2/g]
TM1	U	89.1	4.586	27.7
	HA	87.5	5.513	41.7
	NA	86.9	4.815	33.9
TM2	U	92.4	4.928	26.7
	HA	86.5	5.369	27.8
	NA	86.9	5.069	25.1
TM3	U	89.4	4.422	73.4
	HA	94.9	7.714	70.2
	NA	93.0	5.843	69.8

Table 7
Average results of mold development on the surface of the artificially aged systems.

System (S)	Type of inocula	Mold development			
		Week 1	Week 2	Week 3	Week 4
S1	Natural	0.00	0.00	0.00	0.67 ± 0.58
	Artificial	0.00	0.33 ± 0.58	0.67 ± 0.58	1.33 ± 0.58
S2	Natural	0.00	0.00	0.00	0.33 ± 0.58
	Artificial	0.00	0.00	0.33 ± 0.58	0.67 ± 0.58
S3	Natural	0.00	0.00	0.00	0.33 ± 0.58
	Artificial	0.00	0.00	0.33 ± 0.58	0.67 ± 0.58
Control	Natural	2.67 ± 0.58	3.33 ± 0.58	3.67 ± 0.58	4.00
	Artificial	3.00	3.67 ± 0.58	4.00	4.00

Classification scale: 0 – no growth; 1 – traces of growth; 2 – light growth; 3 – moderate growth; 4 – heavy growth.

4. Discussion

Based on the Coffin-Manson equation [49,50], acceleration factors of 166.4 and 343 were calculated considering the heat/rain and the heat/cold cycles, respectively. Therefore, the accelerated aging procedure adopted in the present study (i.e., ~13 days of heat/rain cycles and 5 days of heat/cold cycles) corresponds approximately to 11 years of natural aging in the urban site in Lisbon, Portugal.

Results showed that all systems presented values of 1 h capillary water absorption lower than 1 kg/m^2, in accordance with the European guideline recommendation for ETICS [26]. However, capillary absorption results were significantly higher after accelerated aging, especially in the acrylic-based system S3 (with an aerogel thermal mortar), which is a non-commercialized product. These results can be attributed to the significant degradation observed in the finishing coats of the artificially aged systems [41,52] (i.e., microcracking, material loss, and in some cases disintegration of the coating with the formation of surface voids), as shown by the SEM-EDS analysis, and to the lack of compatibility between the rendering system and the thermal mortar. The results align with previous studies on multilayer insulation systems with thermal insulation boards [41,62], demonstrating a considerable increase of capillary water absorption after aging. This effect was primarily attributed to surface cracking and occasional paint loss [62,63]. In fact, the acrylic-based finishing coats of the artificially aged systems are no longer capable of effectively protecting the thermal mortars against weathering after ~11 years of aging. Moreover, the capillary water absorption of the thermal mortars was also significantly higher after accelerated aging, especially in the case of the aerogel mortar (TM3). In accordance with previous studies (e.g., Ref. [53]), this can be due to a structural damage occurring in the mortar caused by the hygric stresses during the accelerated aging procedure (i.e., wetting and drying cycles), also leading to an increase of the median pore diameter of the mortar [22]. It can thus be concluded that the capillary water absorption performance of the thermal mortar after accelerated aging strongly influences the capillary water performance of the complete artificially aged system.

On the other hand, different trends can be observed considering the naturally aged systems. After one year of outdoor exposure, acrylic-based systems S2 and S3 presented significantly higher and significantly lower values of capillary water absorption when compared to unaged and artificially aged conditions, respectively. However, greater values of water absorption were obtained after one year of natural aging in the case of system S1, when compared to the results achieved after

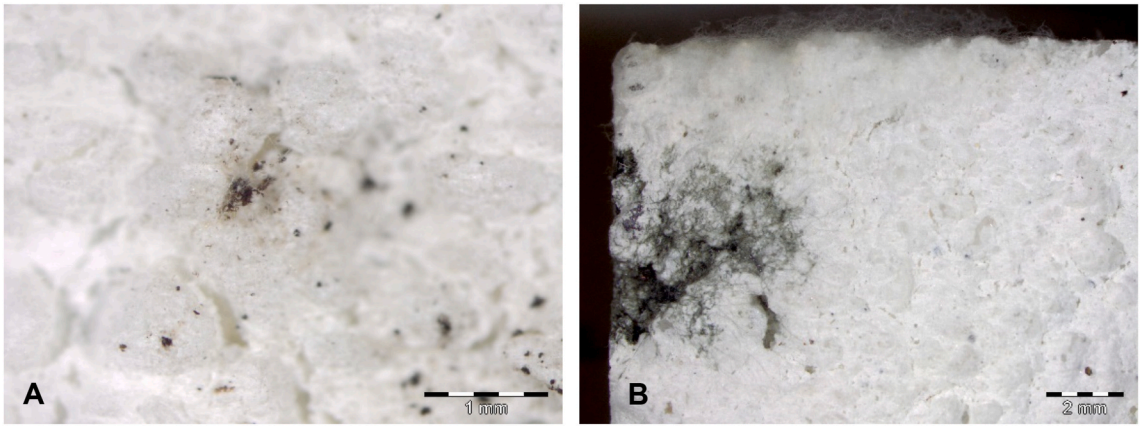

Fig. 19. *A. niger* growth on the surface of the artificially aged system S2 with artificial inocula (A) and biological growth on the surface of the artificially aged system S1 with natural inocula (B).

Table 8
Average results of mold development on the unaged and artificially aged thermal mortars.

Thermal mortar (TM)	Aging condition	Type of inocula	Mold development			
			Week 1	Week 2	Week 3	Week 4
TM1	Unaged	Natural	0.00	0.33 ± 0.58	0.33 ± 0.58	1.00 ± 1.00
		Artificial	0.00	0.00	0.33 ± 0.58	0.67 ± 0.58
	Artificially aged	Natural	0.00	0.00	0.00	0.33 ± 0.58
		Artificial	0.00	0.00	0.33 ± 0.58	0.67 ± 0.58
TM2	Unaged	Natural	0.00	0.00	0.33 ± 0.58	1.00
		Artificial	0.00	0.00	0.00	0.00
	Artificially aged	Natural	0.00	0.00	0.00	0.67 ± 0.58
		Artificial	0.00	0.00	0.33 ± 0.58	1.00
TM3	Unaged	Natural	0.00	0.00	0.00	0.00
		Artificial	0.00	0.00	0.67 ± 0.58	1.00
	Artificially aged	Natural	0.33 ± 0.58	1.00	1.33 ± 0.58	2.33 ± 0.58
		Artificial	0.00	0.33 ± 0.58	1.00	1.67 ± 0.58
Control	Unaged	Natural	2.00	2.67 ± 0.58	3.33 ± 0.58	4.00
		Artificial	3.33 ± 0.58	3.67 ± 0.58	4.00	4.00
	Artificially aged	Natural	2.67 ± 0.58	3.33 ± 0.58	3.67 ± 0.58	4.00
		Artificial	3.00	3.67 ± 0.58	4.00	4.00

artificial aging (presumably corresponding to approximately 11 years of outdoor exposure). This result may be explained by an earlier chemical and physical degradation of the coating of the naturally aged S1 caused by other degradation agents not included in the artificial aging procedure, such as UV radiation or biological colonization [12,54]. In fact, SEM-EDS analysis showed the presence of biocolonization in the surface of the one year naturally aged S1. Moreover, these specimens had higher capillary water absorption and also a slower drying process (i.e., lower DR1 and DR2), if compared to artificially aged specimens, thus favoring water retention within the system and increasing the biocolonization risk [40,44].

The water vapor permeability of the systems was significantly affected after artificial aging, with the highest decrease of the water vapor diffusion resistance coefficient (meaning increase of water vapor permeability) obtained for the acrylic-based system S1, in accordance with the drying kinetics results (i.e., higher DR's after artificial aging). The same trend was also observed for the artificially aged systems S2 and S3, showing an unfavorable increase of capillary water absorption after aging but, at the same time, a favorable increase of water vapor permeability. In fact, a good balance between water intake and drying should be guaranteed, i.e., $A_w \times s_d$ must be as low as possible to ensure hygric compatibility [20,30]. As previously mentioned, the one year naturally aged systems showed a more unfavorable hygric performance, with significantly higher A_w and lower water vapor permeability when compared to the artificially aged systems.

Susceptibility to biological colonization test results showed only traces of growth (i.e., less than 10% of contaminated surface) in the artificially and one year naturally aged systems, most probably due to the biocide incorporated in the acrylic-based paint applied as finishing coat [55]. However, previous studies showed that the efficacy of biocides decreases over time [56,57], with exposure conditions and surface hydrophobicity assuming the main role in avoiding long-term biological colonization [58]. In fact, results showed the difficulty in reproducing several degradation agents and mechanisms in laboratorial conditions, with artificially aged systems (presumably corresponding to 11 years of natural aging) obtaining similar biological growth when compared to naturally aged systems (after one year of outdoor exposure). Additionally, concerning the naturally aged systems, biological growth was slightly higher in systems facing North, with traces of growth detected just after 6 months of aging. These results can be explained by the significantly lower solar radiation received by the specimens oriented towards North, thus leading to lower surface temperatures and increasing the risk of surface condensation and biocolonization [59,60]. Indeed, surface condensation was frequently detected on the naturally aged specimens in the early morning and especially on those facing North. Aesthetic alterations were also more pronounced in North-oriented specimens after 3 months of exposure, with significantly lower surface gloss and a darker tone. On the other hand, results confirmed that color change cannot be detected in the artificially aged systems ($\Delta E^*_{lab} < 2$), reaching values greater than 2 CIELAB units after 3 months of natural aging due to the action of other degradation agents (i.e., pollutants, UV radiation) not included in the accelerated aging [45,61].

5. Conclusions

The use of innovative thermal insulating mortars in multilayer thermal wall systems has been increasing in the last few years, mainly due to their improved thermal performance. Therefore, the existence of

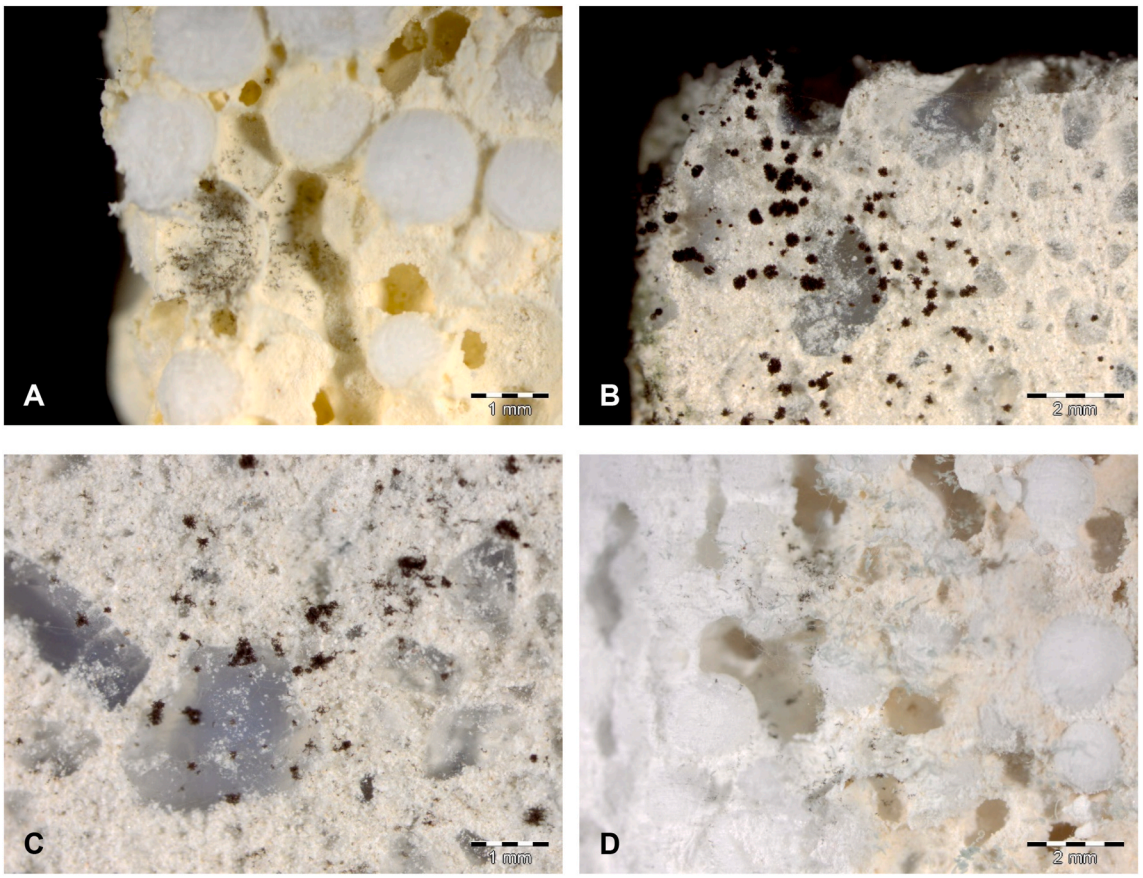

Fig. 20. Biological growth on EPS TM1 (natural inocula) in unaged conditions (A); *A. niger* growth on aerogel TM3 (artificial inocula) in artificially aged (B) and unaged (C) conditions; biological growth on EPS TM2 (natural inocula) in artificially aged conditions (D).

Table 9
Average results of mold development on the surface of the naturally aged systems.

System (S)	Orientation	Mold development			
		3 months	6 months	9 months	12 months
S1	North	0.00	0.33 ± 0.58	0.67 ± 0.58	1.33 ± 0.58
	South	0.00	0.00	0.33 ± 0.58	0.33 ± 0.58
S2	North	0.00	0.33 ± 0.58	1.00	1.00
	South	0.00	0.00	0.33 ± 0.58	0.33 ± 0.58
S3	North	0.00	0.33 ± 0.58	0.67 ± 0.58	1.00
	South	0.00	0.00	0.00	0.33 ± 0.58

reliable data and consistent knowledge related to the performance and durability of these systems is vital to increase their efficiency and sustainability and allow a wider diffusion of this energy efficient constructive solution. In this study, the durability of three multilayer insulation systems incorporating thermal mortars with EPS aggregates and silica aerogel granules was assessed after accelerated aging and one year of natural aging at an urban site in Lisbon, Portugal. The results showed that different trends can be obtained considering diverse rendering system (i.e., base coat + finishing coat) formulations and thermal mortar compositions. The main conclusions are the following:

1) Using the Coffin-Manson equation, the hygrothermal accelerated aging procedure described in the guideline for European technical approval of ETICS (approximately 13 days of heat/rain cycles and 5 days of heat/cold cycles) and adopted in the present study corresponds approximately to 11 years of natural aging in Lisbon, Portugal.
2) The capillary water absorption results were significantly higher after accelerated aging, with the highest increase observed in the case of the non-commercialized acrylic-based system with an aerogel mortar and the lowest for the commercially available acrylic-based system with a lime-based EPS mortar. In fact, the finishing coats of the three systems were substantially affected by the accelerated aging procedure, showing vast microcracking, material loss, and in some cases disintegration with the formation of surface voids. A lack of compatibility between the rendering system and the aerogel-based mortar was also observed. Indeed, after accelerated aging, the acrylic-based finishing coats are no longer capable of protecting the aged systems against liquid water penetration, thus allowing the presence of water in the thermal insulating mortars and affecting the durability of the whole system. Moreover, accelerated aging also affected the water performance of the thermal mortars, with significantly higher capillary water absorption registered for the artificially aged mortars, especially in the case of the non-commercialized mortar with mixed binders and silica aerogel.
3) After one year of outdoor exposure, different trends were observed considering the capillary water absorption of the aged multilayer systems. As expected, acrylic-based systems S2 (with an EPS-based mortar) and S3 (with an aerogel-based mortar) obtained significantly lower capillary water absorption values when compared to the corresponding artificially aged systems. However, greater values of

water absorption were obtained after one-year of aging for the acrylic-based system S1 (with an EPS mortar), when compared to the results obtained after artificially aging (~11 years of outdoor exposure). In fact, results showed an earlier chemical and physical degradation of the coating of the naturally aged S1 caused by additional degradation agents not included in the artificial aging procedure (UV radiation or biological colonization), as shown by the SEM-EDS analysis. The unfavorable balance between capillary water absorption and drying in the case of the naturally aged S1 favored water retention within the system and increased biological colonization.

4) The water vapor permeability and the drying capacity of the systems were significantly affected after artificial aging, with an unfavorable increase of water absorption but, at the same time, a favorable increase of vapor permeability and drying. The one-year naturally aged systems showed a more unfavorable hygric performance, showing significantly higher A_w and lower water vapor permeability when compared to the artificially aged systems. A good balance between water intake and drying is fundamental in these systems to ensure hygric compatibility and prevent further anomalies.
5) Surface gloss was significantly lower after accelerated aging and 3 and 6 months of natural aging facing North and South, respectively. In fact, aesthetic alteration was more pronounced in systems oriented towards North at an early stage. Substantial color change ($\Delta E^*_{lab} > 2$) was detected in all systems after 3 months of natural aging. However, color change cannot be detected after accelerated aging. The results confirmed the difficulty in reproducing the synergistic effect of several degradation agents and mechanisms in laboratorial conditions.
6) Traces of biocolonization (<10% of contaminated area) were observed in both the artificially and naturally aged systems. Nevertheless, results were considerably higher for the aged mortars tested alone, regardless of the type of inocula (artificial or natural). It can be concluded that an enhanced performance of the rendering system is essential to avoid biocolonization in the thermal mortar and therefore in the complete multilayer system.

The results showed a significant increase of capillary water absorption after accelerated aging. This was attributed to a notable deterioration in the performance of the finishing coats after aging, marked by extensive microcracking, material loss, and, in some cases, disintegration with the formation of surface voids. Considering that water ranks among the most detrimental degradation agents of façade coatings, such changes significantly affect the performance and durability of these systems. This could potentially lead to alterations in the thermal performance of the building envelope, an increased risk of biological colonization, aesthetic alterations, and a compromised widespread adoption of this building technology. Furthermore, the results revealed unfavorable hygric performance of the systems after natural aging, characterized by significantly higher water absorption and lower water vapor permeability. This increased water retention within the systems results in additional anomalies, such as biological colonization, cracks, and stains. Aesthetic alteration, including surface gloss and color change, were notably more pronounced in the naturally aged systems, likely due to the substantial accumulation of dirt and dust on the system's surfaces. This accumulation contributes to fungal development, as fungal spores dispersed in the air easily reach the system's surfaces, finding cracks and organic dirt to attach to, along with favorable moisture conditions for spore germination. This, in turn, contributes to further degradation of the systems, including discoloration, loss of cohesion, and the enlargement of crevices, potentially associated with chemical and mechanical anomalies.

The present study provided important results to obtain a reliable dataset on the performance and long-term durability of multilayer insulation systems with thermal insulating mortars that can be used in risk assessment analysis. The results showed similar performance trends considering the artificially and naturally aged systems, showing a significant increase of both capillary water absorption and drying capacity, extensive surface microcracking, traces of biological growth and aesthetic alterations. Nevertheless, according to the Coffin-Manson equation, the accelerated aging procedure corresponds to ~11 years of natural exposure. Therefore, a significantly higher loss of performance would be expected after hygrothermal accelerated aging. However, this was not the case regarding the performance of some of the tested multilayer systems (e.g., capillary water absorption of system S1). It can thus be concluded that the possible synergistic effects of other degradation agents (e.g., UV radiation, biological colonization) not included in the accelerated aging procedure have a significant influence on the long-term durability of the multilayer insulation systems. Despite the difficulty in reproducing these effects in laboratorial conditions, important degradation agents identified in long-term field exposure should be considered in optimized accelerated aging procedures.

CRediT authorship contribution statement

João L. Parracha: Conceptualization, Formal analysis, Funding acquisition, Investigation, Methodology, Validation, Visualization, Writing – original draft, Writing – review & editing. **Rosário Veiga:** Conceptualization, Funding acquisition, Resources, Supervision, Writing – review & editing. **Lina Nunes:** Conceptualization, Funding acquisition, Resources, Supervision, Writing – review & editing. **Inês Flores-Colen:** Conceptualization, Funding acquisition, Supervision, Writing – review & editing.

Declaration of competing interest

The authors declare that they have no known competing financial interests or personal relationships that could have appeared to influence the work reported in this paper.

Data availability

Data will be made available on request.

Acknowledgements

The authors acknowledge CERIS research unit (UIDB/04625/2020), LNEC's Project "Reuse – Coatings for rehabilitation: safety and sustainability" and the Portuguese Foundation for Science and Technology (FCT) for funding research project WGB_Shield (PTDC/ECI-EGC/30681/2017) and the Ph.D. scholarship of the first author (2020.05180.BD). Saint-Gobain and Secil are also acknowledged for the material supply, as well as Prof. Amélia Dionísio (CERENA – IST) for the equipment used in the gloss and color measurements.

References

[1] United Nations Environment Programme, Global status report for buildings and construction: towards a zero-emission, in: Efficient and Resilient Buildings and Construction Sector, Nairobi, 2021, 2021.
[2] Directive EU 2018/844 of the European parliament and of the council of 30 may 2018 amending directive 2010/31/EU on energy performance of buildings and directive 2012/27/EU on energy efficiency, Off. J. Eur. Union (2018).
[3] J.L. Parracha, R. Veiga, I. Flores-Colen, L. Nunes, Toward the sustainable and efficient use of External Thermal Insulation Composite Systems (ETICS): a comprehensive review of anomalies, performance parameters, requirements and durability, Buildings 13 (2023) 1664, https://doi.org/10.3390/buildings13071664.
[4] M. Ganobjak, S. Brunner, J. Wernery, Aerogel materials for heritage buildings: materials, properties and case studies, J. Cult. Herit. 42 (2020) 81–98, https://doi.org/10.1016/j.culher.2019.09.007.
[5] M. Posani, R. Veiga, V.P. de Freitas, Thermal mortar-based insulation solutions for historic walls: an extensive hygrothermal characterization of materials and systems, Construct. Build. Mater. 315 (2022) 125640, https://doi.org/10.1016/j.conbuildmat.2021.125640.

[6] J.L. Parracha, A.R. Santos, R. Lazera, I. Flores-Colen, M.G. Gomes, A. Moret Rodrigues, Performance of lightweight thermal insulating mortars applied on brick substrate specimens and prototype wall, Construct. Build. Mater. 364 (2023) 129954, https://doi.org/10.1016/j.conbuildmat.2022.129954.

[7] C.H. Koh, K. Schollbach, F. Gauvin, H.J.H. Brouwers, Aerogel composite for cavity wall rehabilitation in The Netherlands: material characterization and thermal comfort assessment, Build. Environ. 224 (2022) 109535, https://doi.org/10.1016/j.buildenv.2022.109535.

[8] Z. Pavlík, M. Pavlíková, M. Záleská, M. Vysvaril, T. Zizlavský, Lightweight thermal efficient repair mortars with expanded glass (EG) for repairing historical buildings: the effect of binder type and EG aggregate dosage on their performance, Energy Build. 276 (2022) 112526, https://doi.org/10.1016/j.enbuild.2022.112526.

[9] A. Brás, F. Gonçalves, P. Faustino, Cork-based mortars for thermal bridges correction in a dwelling: thermal performance and cost evaluation, Energy Build. 72 (2014) 296–308, https://doi.org/10.1016/j.enbuild.2013.12.022.

[10] M.G. Gomes, I. Flores-Colen, H. Melo, A. Soares, Physical performance of industrial and EPS and cork experimental thermal insulation renders, Construct. Build. Mater. 198 (2019) 786–795, https://doi.org/10.1016/j.conbuildmat.2018.11.151.

[11] P.F.B. Becker, C. Effting, A. Schackow, Lightweight thermal insulating coating mortars with aerogel, EPS, and vermiculite for energy conservation in buildings, Cement Concr. Compos. 125 (2022) 104283, https://doi.org/10.1016/j.cemconcomp.2021.104283.

[12] J.L. Parracha, G. Borsoi, I. Flores-Colen, R. Veiga, L. Nunes, Impact of natural and artificial ageing on the properties of multilayer external wall thermal insulation systems, Construct. Build. Mater. 317 (2022) 125834, https://doi.org/10.1016/j.conbuildmat.2021.125834.

[13] M. Lazón, P.A. Gracía-Ruiz, Lightweight cement mortars: advantages and inconveniences of expanded perlite and its influence on fresh and hardened state and durability, Construct. Build. Mater. 22 (2008) 1798–1806, https://doi.org/10.1016/j.conbuildmat.2007.05.006.

[14] K.H. Mo, H.J. Lee, M.Y.J. Liu, T.C. Ling, Incorporation of expanded vermiculite lightweight aggregate in cement mortar, Construct. Build. Mater. 179 (2018) 302–306, https://doi.org/10.1016/j.conbuildmat.2018.05.219.

[15] A. Arizzi, G. Cultrone, Aerial lime-based mortars blended with a pozzolanic additive and different admixtures: a mineralogical, textural and physical-mechanical study, Construct. Build. Mater. 31 (2012) 135–143, https://doi.org/10.1016/j.conbuildmat.2011.12.069.

[16] M. Pedroso, I. Flores-Colen, J.D. Silvestre, M.G. Gomes, L. Silva, L. Ilharco, Physical, mechanical, and microstructural characterisation of an innovative thermal insulating render incorporating silica aerogel, Energy Build. 211 (2020) 109793, https://doi.org/10.1016/j.enbuild.2020.109793.

[17] T. Stahl, S. Brunner, M. Zimmermann, K. Ghazi Wakili, Thermo-hygric properties of a newly developed aerogel based insulation rendering for both exterior and interior applications, Energy Build. 44 (2012) 114–117, https://doi.org/10.1016/j.enbuild.2011.09.041.

[18] J. Maia, N.M.M. Ramos, R. Veiga, A new durability assessment methodology of thermal mortars applied in multilayer rendering systems, Construct. Build. Mater. 222 (2019) 654–663, https://doi.org/10.1016/j.conbuildmat.2019.06.178.

[19] EAD 040427-00-0404, Kits for External Thermal Insulation Composite System (ETICS) with a Mortar as Thermal Insulation Product and Renderings or Discontinuous Claddings as Exterior Skin, Guideline for European Technical Approval, EOTA (European Organisation for Technical Approval), 2019.

[20] M. Posani, R. Veiga, V. Freitas, Thermal renders for traditional and historic masonry walls: comparative study and recommendations for hygric compatibility, Build. Environ. 228 (2023) 109737, https://doi.org/10.1016/j.buildenv.2022.109737.

[21] J. Maia, M. Pedroso, N.M.M. Ramos, I. Flores-Colen, P.F. Pereira, L. Silva, Durability of a new thermal aerogel-based rendering system under distinct accelerated aging conditions, Materials 14 (18) (2021) 5413, https://doi.org/10.3390/ma14185413.

[22] H. Xiong, K. Yuan, J. Xu, M. Wen, Pore structure, adsorption, and water absorption of expanded perlite mortar in external thermal insulation composite system during aging, Cement Concr. Compos. 116 (2021) 103900, https://doi.org/10.1016/j.cemconcomp.2020.103900.

[23] M. Pedroso, I. Flores-Colen, J.D. Silvestre, M.G. Gomes, L. Silva, P. Sequeira, J. de Brito, Characterisation of a multilayer external wall thermal insulation system. Application in a Mediterranean climate, J. Build. Eng. 30 (2020) 101265, https://doi.org/10.1016/j.jobe.2020.101265.

[24] EN 998-1:2017, Specification for Mortar for Masonry - Part 1: Rendering and Plastering Mortar, European Committee for Standardization, 2017.

[25] NP EN 1584:2019, Specifications for External Renders and Internal Plasters Based on Organic Binders, Instituto Português da Qualidade, 2019 (in Portuguese).

[26] EAD 040083-00-0404, External Thermal Insulation Composite Systems with Rendering. Guideline for European Technical Approval, EOTA (European Organisation for Technical Approval), 2020.

[27] EN 16322:2013, Conservation of Cultural Heritage – Test Methods – Determination of Drying Properties, European Committee for Standardisation, Brussels, Belgium, 2013.

[28] EN 1015-19:2008, Methods of Test for Mortar for Masonry – Part 19: Determination of Water Vapour Permeability of Hardened Rendering and Plastering Mortars, European Committee for Standardisation, Brussels, Belgium, 2008.

[29] W. Mokrzycki, M. Tatol, Color difference Delta E-A survey, Mach. Graph. Vis. 20 (4) (2011) 383–411.

[30] J.L. Parracha, G. Borsoi, I. Flores-Colen, R. Veiga, L. Nunes, A. Dionísio, M. G. Gomes, P. Faria, Performance parameters of ETICS: correlating water resistance, bio-susceptibility and surface properties, Construct. Build. Mater. 272 (2021) 121956, https://doi.org/10.1016/j.conbuildmat.2020.121956.

[31] ASTM D5590-17:2017, Determining the Resistance of Paint Films and Related Coatings to Fungal Defacement by Accelerated Four-Week Agar Plate Assay, ASTM International, Pennsylvania, USA, 2017.

[32] W. Brown, J. Ullet, A. Karagiozis, T. Tonyan, Barrier EIFS clad walls: results from moisture engineering study, J. Therm. Insul. Build. Envelopes 20 (1997) 206–226, https://doi.org/10.1177/109719639702000304.

[33] H. Hens, J. Carmeliet, Performance prediction for masonry walls with EIFS using calculation procedures and laboratory testing, J. Therm. Insul. Build. Envelopes 25 (2002) 167–187, https://doi.org/10.1106/109719602024141.

[34] E. Barreira, V.P. de Freitas, Experimental study of the hygrothermal behaviour of external thermal insulation composite systems (ETICS), Build. Environ. 63 (2013) 31–39, https://doi.org/10.1016/j.buildenv.2013.02.001.

[35] M. D'Orazio, G. Cursio, L. Graziani, L. Aquilanti, A. Osimani, F. Clementi, C. Yéprémian, V. Lariccia, S. Amoroso, Effects of water absorption and surface roughness on the bioreceptivity of ETICS compared to clay bricks, Build. Environ. 77 (2014) 20–28, https://doi.org/10.1016/j.buildenv.2014.03.018.

[36] A.S. Silva, G. Borsoi, J.L. Parracha, I. Flores-Colen, R. Veiga, P. Faria, A. Dionísio, Evaluating the effectiveness of self-cleaning products applied on external thermal insulation composite systems (ETICS), J. Coating Technol. Res. 19 (2022) 1437–1448, https://doi.org/10.1007/s11998-022-00617-x.

[37] J.V. Koleske, R. Springate, D. Brezinski, Additives Handbook 2011, Paint and Coatings Industry, 2011.

[38] G. Liu, H. Xia, Y. Niu, X. Zhao, G. Zhang, L. Song, H. Chen, Fabrication of self-cleaning photocatalytic durable building coating based on WO_3-TNs/PDMS and NO degradation performance, Chem. Eng. J. 409 (2021) 128187, https://doi.org/10.1016/j.cej.2020.128187.

[39] C.C. Gaylarde, L.H.G. Morton, K. Loh, M.A. Shirakawa, Biodeterioration of external architectural paint films – a review, Int. Biodeterior. Biodegrad. 65 (2011) 1189–1198, https://doi.org/10.1016/j.ibiod.2011.09.005.

[40] A.-L. Pasanen, J.-P. Kasanen, S. Rautiala, M. Ikäheimo, J. Rantamäki, H. Kääriäinen, P. Kalliokoski, Fungal growth and suvival in building materials under fluctuating moisture and temperature conditions, Int. Biodeterior. Biodegrad. 46 (2) (2000) 117–127, https://doi.org/10.1016/S0964-8305(00)00093-7.

[41] J.L. Parracha, G. Borsoi, R. Veiga, I. Flores-Colen, L. Nunes, C.A. Viegas, L. M. Moreira, A. Dionísio, P. Faria, Durability assessment of external thermal insulation composite systems in urban and maritime environments, Sci. Total Environ. 849 (2022) 157828, https://doi.org/10.1016/j.scitotenv.2022.157828.

[42] M. Klamer, E. Morsing, T. Husemoen, Fungal growth on different insulation materials exposed to different moisture regimes, Int. Biodeterior. Biodegrad. 54 (4) (2004) 277–282, https://doi.org/10.1016/j.ibiod.2004.03.016.

[43] E. Jerábková, D. Tesarová, Resistance of various materials and coatings used in wood constructions to growth of microorganisms, Wood Res. 63 (2018) 993–1002.

[44] C. Ferrari, G. Santunione, A. Libbra, A. Muscio, E. Sgarbi, C. Siligardi, G.S. Barozzi, Review on the influence of biological deterioration on the surface properties of building materials: organisms, materials, and methods, Int. J. Des. Nat. Ecodyn. 10 (1) (2015) 21–39, https://doi.org/10.2495/DNE-V10-N1-21-39.

[45] H.K. Tanaca, C.M.R. Dias, C.C. Gaylarde, V.M. John, M.A. Shirakawa, Discoloration and fungal growth on three fiber cement formulations exposed in urban, rural and coastal zones, Build. Environ. 46 (2011) 324–330, https://doi.org/10.1016/j.buildenv.2010.07.025.

[46] J. Bochen, S. Gil, Properties of pore structure of thin-layer external plasters under ageing in simulated environment, Construct. Build. Mater. 23 (2009) 2958–2963, https://doi.org/10.1016/j.conbuildmat.2009.02.041.

[47] I. Mandilaras, I. Atsonios, G. Zannis, M. Founti, Thermal performance of a building envelope incorporating ETICS with vacuum insulation panels and EPS, Energy Build. 85 (2014) 654–665, https://doi.org/10.1016/j.enbuild.2014.06.053.

[48] M. Posani, M.R. Veiga, V.P. de Freitas, Towards resilience and sustainability for historic buildings: a review of envelope retrofit possibilities and a discussion on hygric compatibility of thermal insulations, Int. J. Architect. Herit. 15 (5) (2021) 807–823, https://doi.org/10.1080/15583058.2019.1650133.

[49] B.P. Jelle, Accelerated climate ageing of building materials, components and structures in the laboratory, J. Mater. Sci. 47 (2012) 6475–6496, https://doi.org/10.1007/s10853-012-6349-7.

[50] U. Berardi, R.H. Nosrati, Long-term thermal conductivity of aerogel-enhanced insulating materials under different laboratory aging conditions, Energy 147 (2018) 1188–1202, https://doi.org/10.1016/j.energy.2018.01.053.

[51] Delserro engineering solutions, in: Temperature Cycling Testing: Coffin-Mason Equation, 2015. http://www.desolutions.com/blog/2014/10/temperature-cycling-testing-coffin-manson-equation/.

[52] J. Maia, N.M.M. Ramos, R. Veiga, Assessment of test methods for the durability of thermal mortars exposure to freezing, Mater. Struct. 52 (2019) 112, https://doi.org/10.1617/s11527-019-1411-4.

[53] A.N. Karim, P. Johansson, A.S. Kalagasidis, Increasing water absorptivity of an aerogel-based coating mortar in subsequent wetting and drying, Gels 8 (2022) 764, https://doi.org/10.3390/gels8120764.

[54] M.A. Shirakawa, K. Loh, V.M. John, M.E.S. Silva, C.C. Gaylarde, Biodeterioration of painted mortar surfaces in tropical urban and coastal situations: comparison of four paint formulations, Int. Biodeterior. Biodegrad. 65 (2011) 669–674, https://doi.org/10.1016/j.ibiod.2011.03.004.

[55] F. Reiß, N. Kiefe, M. Noll, S. Kalkhof, Application, release, ecotoxicological assessment of biocide in building materials and its soil microbial response, Ecotoxicology and Environmental Science 224 (2021) 112707, https://doi.org/10.1016/j.ecoenv.2021.112707.

[56] W. Hofbauer, N. Krueger, F. Mayer, K. Breuer, Biocide tolerance in microorganisms with respect to the durability of building coatings. In Proceedings of XII DBMC – International Conference on Durability of Building Materials and Components, Porto, Portugal. pp. 93-99. 12-15 April.
[57] M. Burkhardt, S. Zuleeg, R. Vonbank, P. Schmidt, S. Hean, X. Lamani, K. Bester, M. Boller, Leaching of additives from construction materials to urban stormwater runoff, Water Sci. Technol. 63 (2011) 1974–1982, https://doi.org/10.2166/wst.2011.128.
[58] M.A. Shirakawa, R.G. Tavares, C.C. Gaylarde, M.E.S. Taqueda, K. Loh, V.M. John, Climate as the most important factor determining anti-fungal biocide performance in paint films, Sci. Total Environ. 408 (2010) 5878–5886, https://doi.org/10.1016/j.scitotenv.2010.07.084.
[59] E. Barreira, V.P. de Freitas, External thermal insulation composite systems: critical parameters for surface hygrothermal behaviour, Adv. Mater. Sci. Eng. (2014) 650752, https://doi.org/10.1155/2014/650752.
[60] H. Barberousse, R.J. Lombardo, G. Tell, A. Couté, Factors involved in the colonisation of building façades by algae and cyanobacteria in France, Biofouling 22 (2006) 69–77, https://doi.org/10.1080/08927010600564712.
[61] M.V. Diamanti, R. Paolini, M. Rossini, A.B. Aslan, M. Zinzi, T. Poli, M.P. Pedeferri, Long term self-cleaning and photocatalytic performance of anatase added mortars exposed to the urban environment, Construct. Build. Mater. 96 (2015) 270–278, https://doi.org/10.1016/j.conbuildmat.2015.08.028.
[62] R. Landolfi, M. Nicolella, Durability assessment of ETICS: comparative evaluation of different insulating materials, Sustainability 14 (2022) 980, https://doi.org/10.3390/su14020980.
[63] J. Slusarek, B. Orlik-Kozdón, J. Bochen, T. Muzyczuk, Impact of the imperfection of thermal insulation on structural changes of thin-layer façade claddings in ETICS, J. Build. Eng. 32 (2020) 101487, https://doi.org/10.1016/j.jobe.2020.101487.
[64] G. Griciute, R. Bliudzius, R. Norvaisiene, The durability test method for external thermal insulation composite system used in cold and wet climate countries, J. Sustain. Architect. Civ. Eng. 1 (2) (2013) 50–56, https://doi.org/10.5755/j01.sace.1.2.2778.
[65] B. Daniotti, R. Paolini, Experimental programme to assess ETICS cladding durability, in: 11 DBMC International Conference on Durability of Building Materials and Components, Istanbul, Turkey, 2008, pp. 11–14.
[66] L. Addleson, Building Failures: A Guide to Diagnosis, Remedy and Prevention, third ed., Butterworth Architecture, Oxford, England, 1992.
[67] J.L. Parracha, G. Borsoi, R. Veiga, I. Flores-Colen, L. Nunes, A.R. Garcia, L. M. Ilharco, A. Dionísio, P. Faria, Effects of hygrothermal, UV and SO_2 accelerated ageing on the durability of ETICS in urban environments, Build. Environ. 204 (2021) 108151, https://doi.org/10.1016/j.buildenv.2021.108151.